Fracture mechanism simulation of inhomogeneous anisotropic rocks by extended finite element method

Ehsan Mohtarami[a,*], Alireza Baghbanan[a,b], Hamid Hashemolhosseini[c], Stéphane P.A. Bordas[d, e, f]

[a] Department of Mining Engineering, Isfahan University of Technology, Isfahan, Iran

[b] Visiting Professor of Rock Mechanics, Department of Civil Engineering, School of Engineering, Aalto University, Finland

[c] Department of Civil Engineering, Isfahan University of Technology, Isfahan, Iran

[d] Institute of Computational Engineering, University of Luxembourg, Maison du Nombre, 6 Avenue de la Fonte, 4364 Esch-sur-Alzette, Luxembourg

[e] Department of Medical Research, China Medical University Hospital, China Medical University, Taichung, Taiwan

[f] Institute of Mechanics and Advanced Materials, School of Engineering, Cardiff University, UK

Abstract

The vast majority of rock masses is anisotropic due to factors such as layering, unequal in-situ stresses, joint sets, and discontinuities. Meanwhile, given the frequently asymmetric distribution of pores, grain sizes or different mineralogical compounds in different locations, they are often classified as inhomogeneous materials. In such materials, stress intensity factors (SIFs) at the crack tip, which control the initiation of failure, strongly depend on mechanical properties of the material near that area. On the other hand, crack propagation trajectories highly depend on the orthotropic properties of the rock mass. In this study, the SIFs are calculated by means of anisotropic crack tip enrichments and an interaction integral are developed for inhomogeneous materials with the help of the extended finite element method (XFEM). We also use the *T*-stress within the crack tip fields to develop a new criterion to estimate the crack initiation angles and propagation in rock masses. To verify and validate the proposed approach, the results are compared with experimental test results and those reported in the literature. It is found that the ratio of elastic moduli, shear stiffnesses, and material orientation angles have a significant impact on the SIFs. However, the rate of change in material properties is found to have a moderate effect on these factors and a more pronounced effect on the failure force. The results highlight the potential of the proposed formulation in the estimation of SIFs and crack propagation paths in inhomogeneous anisotropic materials.

Keywords: Extended Finite Element Method; stress intensity factor; anisotropic rock; crack trajectory; Hollow Center Cracked Disc; Anisotropic Maximum Tangential Stress.

1. Introduction

There are many defects such as cracks, joints, fissures and fractures in rock structures. Consequently, when a rock is subjected to mechanical loading in different situations, it may fail and local cracks may extend from the tips of preexisting discontinuities. Therefore, understanding of rock failure mechanics plays an important role in addressing a number of important engineering issues. Rock fracture simulation requires computing the stress intensity factors (SIFs), from which the crack propagation trajectory can be simulated. Evaluating SIFs and predicting the crack propagation trajectory are necessary in different fields of rock engineering including hydraulic fracturing, underground excavation, rock mass stability analysis, hydrocarbon reservoirs, and blasting operations [1-6]. However, irregular layering, unequal in-situ stresses, existing of joint sets and discontinuities make rock masses intrinsically anisotropic [7]. In addition, given the asymmetric distribution of pores, grain sizes and the presence of different mineralogical compounds in different locations, rocks are often classified as heterogeneous materials. Robertson [8] states that the distance from a heat source (being at different temperatures) causes variations in rock mechanical properties as a function of location. Moreover, Mohtarami et al. [9] reported that some engineering operations such as acidizing of oil wells, can also intensify the inhomogeneous and anisotropic behavior of geo-materials.

Although most researchers categorize rocks as inhomogeneous anisotropic materials [7, 10], the majority of studies in the rock fracture mechanics have assumed rocks to behave as homogeneous and isotropic materials. For instance, Eftekhari et al. [11] studied the crack initiation angle and propagation path in homogeneous isotropic disk-shaped specimens and then examined the effect of initial crack lengths and angles on a variety of disk-shaped specimens [12, 13]. Aliha et al. [14] studied the size of limestone disk-shaped specimens and showed that the Maximum Tangential Stress (MTS) criterion is not suitable for analysis of crack propagation. The effect of material anisotropy on the mode *I* stress intensity factors (SIFs) by a 3D Finite Element Method was also investigated and reported by Hirose et al. [15]. Recently many attempts have been conducted to characterize the effects of geometric parameters (crack length, crack inclination angle, geometric shape of specimen) and mechanical properties (Poisson's ratio, degree of material anisotropy and anisotropic orientation) in homogeneous anisotropic materials [9, 12, 14, 16-26]. However, the assumption of inhomogeneity and variations in rock mass properties have not been

considered. Researchers argue that the simplified assumption of inhomogeneous isotropic media cannot satisfy the actual conditions of rocks [16, 17, 27]. Furthermore, failure initiation, crack initiation angle and propagation paths in inhomogeneous anisotropic materials strongly depend on mechanical properties of the material near the crack tip and its anisotropy characteristics [9, 17, 18, 20, 28-30]. Several theoretical models [31-35] and experimental techniques [36-40] were developed to investigate the mixed mode crack growth (the combination of opening and shearing modes) in rocks. However, existing theoretical models are limited to simple geometries, load conditions, and materials behaviors.

Nowadays, numerical methods mostly use in engineering and science. To model discontinuities and singularities, the Extended Finite Element Method (XFEM) is a strong contender. The XFEM was initially introduced by Belytschko and Black [41]. Significant improvements in this procedure were introduced by Moës et al. [42] and Dolbow [43]. Bordas et al. [44] provided an XFEM library which is able to solve many problems of fracture mechanics. This method was firstly used to investigate isotropic Functionally Graded Materials (FGMs) by Dolbow and Gosz [45]. In order to take into account the anisotropy in computations, Asadpoure et al. [16, 46, 47] introduced a set of enrichment functions inspired by analytical solutions of Sih et al. [48] and Viola et al. [49] which used the notion of complex numbers. Recently XFEM has been developed to model a 3D crack propagation [50-53] and multi-crack growth [24-26]. In addition, in the field of rock engineering, XFEM is one of the powerful tools that has been successfully applied to simulate hydraulic fracturing in hydrocarbon reservoirs, given the inherent anisotropy of the rock formations [54-56]. The XFEM basic concept is to enrich the solution through a local partition of unity [17]. The fracturing process can be modeled by enriching a polynomial basis with new functions thereby enabling the method to reproduce the (arbitrary) enrichment functions. For example, by employing the discontinuous Heaviside function, crack surfaces can be modeled without being considered as geometric boundaries i.e. without meshing our re-meshing process. Also, the singularity of the stress field can be reproduced by the use of appropriate asymptotic displacement functions. This study is an attempt to provide an accurate simulation of failure mechanisms of an inhomogeneous anisotropic rock material. For this purpose, obtaining anisotropic enrichment functions, incorporating inhomogeneity into the formulations, and determining a criterion for accurate prediction of crack trajectory are necessary. To overcome these problems, we need to employ precise analytical solutions in the XFEM context.

To our knowledge, the first analytical solution of inhomogeneous materials dates back to 1960s, when Gibson [57] modeled soil as an inhomogeneous material. Atkinson [58], Dhaliwal and Singh [59], Delale and Erdogan [60] analyzed the cracking problem of inhomogeneous materials through a variable modulus of elasticity. Delale and Erdogan [60] showed that the order of singularity of the stress field near a crack tip in non-homogeneous materials is of order -1/2 (i.e., $O(r^{-1/2})$), as it is for homogeneous materials. Since the mechanical properties of inhomogeneous materials vary with location, the applied analysis method should be able to account for these variations at any desired point. Recently, Kim and Paulino [61] analyzed the mixed mode failure of inhomogeneous FGMs by using finite element approach with a path independent J_k^* integral, a modified crack closure integral method, and a displacement correction technique. The interaction integral for homogeneous isotropic materials is attributed to Yau et al. [62]. Wang et al. [63] further developed the approach for homogeneous orthotropic materials and this method is robust and accurate for the calculation of SIFs in inhomogeneous materials.

There are several failure criteria in predicting the direction of crack initiation and propagation [24-26]. The Maximum Tangential Stress (MTS) criterion in which a crack propagates from its tip in the direction maximizing the tangential stress has been frequently used to model crack growth in XFEM [64]. However, deviations of results provided by the MTS from experimental results have encouraged the development of alternatives or improvements to this method [14, 65-68]. Eftekhari et al. [21] used a stress-based criterion to introduce an improved MTS theory in the XFEM framework. Smith et al. [69] utilized the *T*-stress as well as singular terms of the crack tip to develop a criterion called the GMTS to predict crack initiation and propagation trajectory in homogeneous isotropic materials. They reported that the mixed mode toughness of a cracked specimen depended on the magnitude and sign of the *T*-stress, a notion that was ignored in previous studies. Aliha and Ayatollahi tested this criterion for a variety of rock specimens with the assumption of homogeneity and isotropy and confirmed its validity [70-72]. They reported that this criterion was capable to predict the crack trajectory. Mohtarami et al. [23] recently developed a crack propagation criterion in anisotropic rocks using the concept of *T*-stress.

The absence of a comprehensive criterion for understanding the failure mechanism of inhomogeneous anisotropic rocks encouraged the authors to investigate the use of extended finite element method simulation to study the effect of inhomogeneity and anisotropy on the failure

mechanism of such rocks. In this case, anisotropic enrichment functions along with a developed interaction integral method for inhomogeneous materials are applied. In addition, the concept of *T*-stress is incorporated into the formulation of the stress field near a crack tip in an inhomogeneous anisotropic material in order to introduce a new criterion called "Inhomogeneous Anisotropic Maximum Tangential Stress (IAMTS)" to predict the crack initiation angle and fracture path in such materials. In three dimensions, incorporating such higher order terms require special treatments proposed recently in [50-52].

Following the concept of T-stress, the method to calculate the stress and the displacement fields near the crack tip in an anisotropic body is described using the solution proposed by Sih et al. [48]. This method is then utilized to develop the MTS criterion for anisotropic solids. In the next stage, the extended finite element method, enrichment functions, and interaction integrals in inhomogeneous anisotropic bodies are developed to show how to reproduce the near tip stresses and to calculate the SIFs. Then, the validity and the accuracy of the proposed method in predicting rock failure mechanisms are investigated. The XFEM simulation results are compared with laboratory experimental test results and provided results in the literature. Due to the availability and simple preparation of core-based specimens in estimating rock fracture toughness, these specimens are mostly used to study rock fracture mechanisms. Therefore, a sensitivity analysis of the geometric and mechanical parameters of an inhomogeneous anisotropic disk-shaped specimen is also addressed.

2. Governing equations in Inhomogeneous Anisotropic materials

Rocks are often formed by gradual cooling and crystallization of magma and experience asymmetric in-situ stresses throughout their lifetime, so that they are typically inhomogeneous and anisotropic materials. The trend of anisotropy and inhomogeneity can be gradual or drastically near a discontinuity. In fact, such variability can be found at all scales, from the microstructural, granular, crystalline through the laboratory upon and to the engineering scales. Hudson and Harrison [7] introduced two acronyms CHILE and DIANE to distinguish traditional simplified assumptions used in rock modeling from actual rock characteristics. A Continuous, Homogeneous, Isotropic and Linearly-Elastic (CHILE) material is one that is most commonly assumed for the purposes of modelling, while a Discontinuous, Inhomogeneous, Anisotropic, Non-Elastic (DIANE) rock is the material which the engineer has to deal with in practice [7].

The linear elastic plane stress fields near the crack tip can be described as symmetric and asymmetric fields called Mode *I* and Mode *II*, respectively. The stresses associated with each field can be expressed as a series expansion of eigenvalues [73]; with general form as follows,

$$\sigma_{ij} = \underbrace{\underbrace{\sin\ gular\ terms\ of}_{stress\ around\ crack\ tip}}_{function\ of\ K_I, K_{II}, r, \theta} + \underbrace{T - stress}_{\substack{appears\ only\ in \\ Mode\ I\ and\ for\ \sigma_{xx}}} + \underbrace{O\left(r^{1/2}\right)}_{Higher\ order\ terms} \tag{1}$$

where x and y are Cartesian coordinates, and r and θ are polar coordinates defined with respect to the crack tip (see Fig. 1). The parameters K_I, and K_{II} are stress intensity factors in mode *I* and *II*, and T is the T-stress, which all depend on the geometry and loading, and can vary significantly from specimen to specimen [69]. Near the crack tip, higher order terms of the series are negligible [74]. In the conventional MTS criterion [31], only the singular term of Eq. (1) is considered, but for the criterion introduced in our model, the impact of both the singular term and the T-stress is considered. Thus, the two terms in the right hand side of Eq. (1) yield the stress fields near the crack tip, and can be used to predict the crack propagation trajectory.

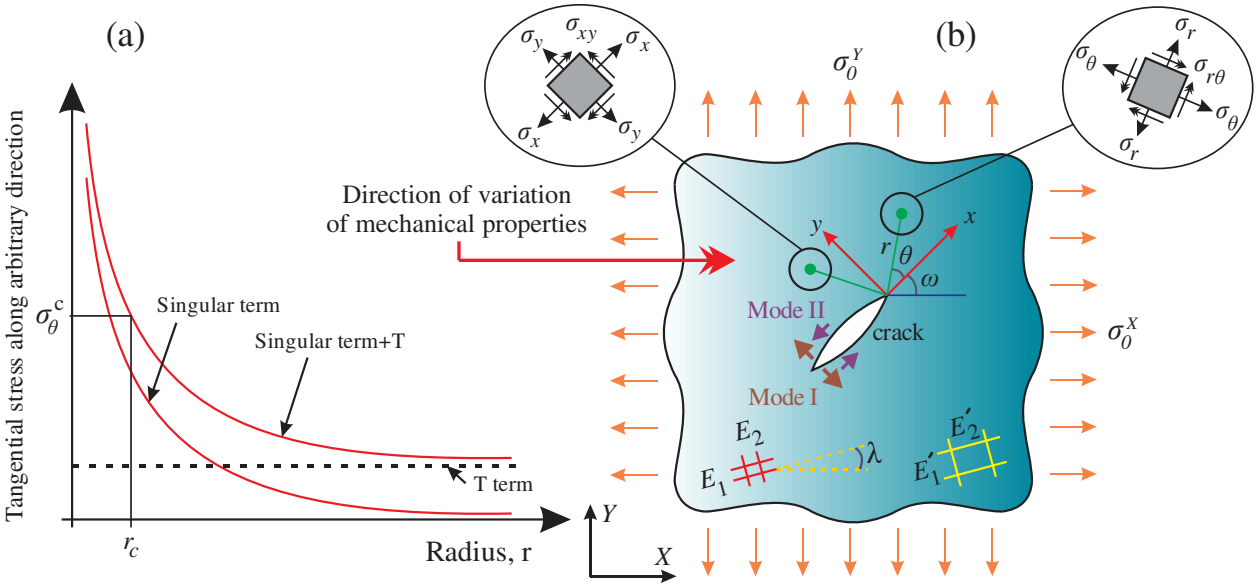

Fig. 1. **(a)** Elastic tangential stress along the direction of fracture initiation [69]; **(b)** an environment with inhomogeneous anisotropic behavior and the respective Cartesian and polar systems.

A constant stress parallel to the crack, term T, appears only due to the symmetrical component of loading, and vanishes in pure mode *II* [75]. Several methods have been developed to calculate term T for different loading conditions and geometries [76-79]. Since the determination of the T-

stress depends on the stress or displacement fields associated with the crack, if the higher precision is considered, the higher *T*-stress is approximated. In the conventional finite element method, this operation is considered by increasing the number of elements of the crack tip zone [80, 81]. The enrichment functions, however, allow the stress singularity and the discontinuity-induced displacements to reproduce accurately without fine mesh generation or re-meshing process. Ayatollahi et al. [75] developed an improved method to obtain *T*-stress by using the displacements along crack surfaces with less dependency on the number of elements. They assert that for a mixed mode *I/II*, term *T* can be expressed as follows,

$$T = \frac{1}{2}E'\left(\left(\frac{du_x}{dx}\right)_{\theta=-\pi} + \left(\frac{du_x}{dx}\right)_{\theta=\pi}\right) \tag{2}$$

where u_x represents the displacement along the x-axis, and E' is defined as follows,

$$E' = \begin{cases} E & \text{plane stress} \\ \dfrac{E}{1-\nu^2} & \text{plane strain} \end{cases} \tag{3}$$

Replacing the slope du_x / dx with displacement values gives [75],

$$T = \frac{1}{2x}E'[u_x(x,-\pi) + u_x(x,\pi)] \tag{4}$$

where x is a small distance from the crack tip. Aliha et al. [14] suggested an optimum value of this parameter as follows,

$$r_c = \frac{1}{2\pi}\left(\frac{K_{IC}}{\sigma_t}\right)^2 \tag{5}$$

where K_{IC} and σ_t are the toughness and the tensile strength of the tested rock, respectively. Smith et al. [69] suggested that within the critical distance r_c, the singular term of Eq. (1) was limited and *T*-stress could be a major contributor to the tangential stress σ_θ (Fig. 1a). The role of *T*-stress on the fracture mechanism of various materials has been previously investigated by several researchers and it has been suggested that *T*-stress has a significant effect on crack trajectory in mixed mode. Generally, positive *T*-stress increases the crack initiation angle, while negative *T*-stress decreases the crack initiation angle. For more details, one can refer to references [23, 82-84].

The singular term of Eq. (1) can be obtained using Sih's solution method [48] for inhomogeneous anisotropic materials. In this method, the problem is solved by expressing stresses

and displacements as complex functions where the real parts should be determined. A cracked inhomogeneous anisotropic medium with material orientation angle λ, arbitrary boundary conditions and loading is shown in Fig. 1b. As can be seen, (X, Y) are considered as the global Cartesian coordinates and (x, y) as the local crack tip Cartesian system that defines the local crack tip in the polar coordinate system (r, θ), when $x+iy=re^{i\theta}$. The term ω is defined as the angle between the local and the global coordinate systems. If boundary stresses σ_0^X and σ_0^Y are applied in the X and Y directions, respectively, the Cartesian stress components (σ_x, σ_y, σ_{xy}) and the polar stress components (σ_r, σ_θ, $\sigma_{r\theta}$) can be calculated for any arbitrary element (see Fig. 1b). In this hypothetical body, the degree of anisotropy at any point is defined as the ratio E_1/E_2 and the intensity of changes in elastic modulus from point to point is known as the pattern of heterogeneity or inhomogeneity order.

In such media, the characteristic equation relating to a fourth order partial differential equation, which results from equilibrium and compatibility conditions, is as follows [85],

$$a_{11}\mu^4 - 2a_{16}\mu^3 + (2a_{12} + a_{66})\mu^2 - 2a_{26}\mu + a_{22} = 0 \tag{6}$$

where a represents components of the fourth order material compliance tensor and is defined as $\varepsilon_\alpha = a_{\alpha\beta}\sigma_\beta$ $(\alpha, \beta = 1,2,6)$ [85]. Lekhnitskii [85] showed that the roots of Eq. (6) were either complex or entirely imaginary, and existed in the form of conjugate pairs μ_1, $\overline{\mu_1}$, μ_2 and $\overline{\mu_2}$. In this case, the stress fields near the crack tip (mixed mode) are as follows,

$$\sigma_{xx}(r,\theta) = \frac{K_I}{\sqrt{2\pi r}} Re\left\{\frac{\mu_1\mu_2}{\mu_1-\mu_2}\left[\frac{\mu_2}{g_2(\theta)} - \frac{\mu_1}{g_1(\theta)}\right]\right\} + \frac{K_{II}}{\sqrt{2\pi r}} Re\left\{\frac{1}{\mu_1-\mu_2}\left[\frac{\mu_2^2}{g_2(\theta)} - \frac{\mu_1^2}{g_1(\theta)}\right]\right\} + T + O\left(r^{1/2}\right) \tag{7a}$$

$$\sigma_{yy}(r,\theta) = \frac{K_I}{\sqrt{2\pi r}} Re\left\{\frac{1}{\mu_1-\mu_2}\left[\frac{\mu_1}{g_2(\theta)} - \frac{\mu_2}{g_1(\theta)}\right]\right\} + \frac{K_{II}}{\sqrt{2\pi r}} Re\left\{\frac{1}{\mu_1-\mu_2}\left[\frac{1}{g_2(\theta)} - \frac{1}{g_1(\theta)}\right]\right\} + O\left(r^{1/2}\right) \tag{7b}$$

$$\sigma_{xy}(r,\theta) = \frac{K_I}{\sqrt{2\pi r}} Re\left\{\frac{\mu_1\mu_2}{\mu_1-\mu_2}\left[\frac{1}{g_1(\theta)} - \frac{1}{g_2(\theta)}\right]\right\} + \frac{K_{II}}{\sqrt{2\pi r}} Re\left\{\frac{1}{\mu_1-\mu_2}\left[\frac{\mu_1}{g_1(\theta)} - \frac{\mu_2}{g_2(\theta)}\right]\right\} + O\left(r^{1/2}\right) \tag{7c}$$

where Re is the real part of the complex term, K_I and K_{II} are the stress intensity factors in mode I and II, the higher order terms are negligible near the crack tip, and parameter g is defined as follows;

$$g_i(\theta) = \sqrt{\cos(\theta) + \mu_i \sin(\theta)} \quad (i = 1,2) \tag{8}$$

It should be noted that in numerical computations for variable material parameters which vary from point to point, crack tip properties are used in calculations.

3. Concept of Extended Finite Element Method

In the XFEM solution, an unknown displacement field is divided into two parts. One part is due to the conventional finite element solution, and the other part is due to the enriched domain, which can be presented as follows,

$$u^h(x) = u^{FEM}(x) + u^{XFEM}(x) = \sum_{j=1}^{n} N_j(x).u_j + \sum_{k=1}^{m} N_k(x).\psi(x).a_k \tag{9}$$

where, ψ is an enrichment function and the a_k are additional degrees of freedom which are added to the nodes whose support is split by the discontinuity, and m and n are number of enriched nodes and total number of nodes, respectively. In Eq. (9), function ψ can represent any specific behavior to be reproduced by the enriched approximation; discontinuities (u^{He}) or/and singularities (u^{tip}),

$$u^h = u^{XFEM} + u^{FEM} = u^{tip} + u^{He} + u^{FEM} \tag{10}$$

In Fig. 2, three aforementioned zones are shown, where u^{tip} is the displacement due to the crack tip enrichment functions, u^{He} is the displacement field due to the domain enriched by the Heaviside function, and u^{FEM} is the displacement due to conventional finite element method. In Fig. 2, blending elements refer to elements that have at least one or more enriched nodes. For more details, one can refer to references [30, 86].

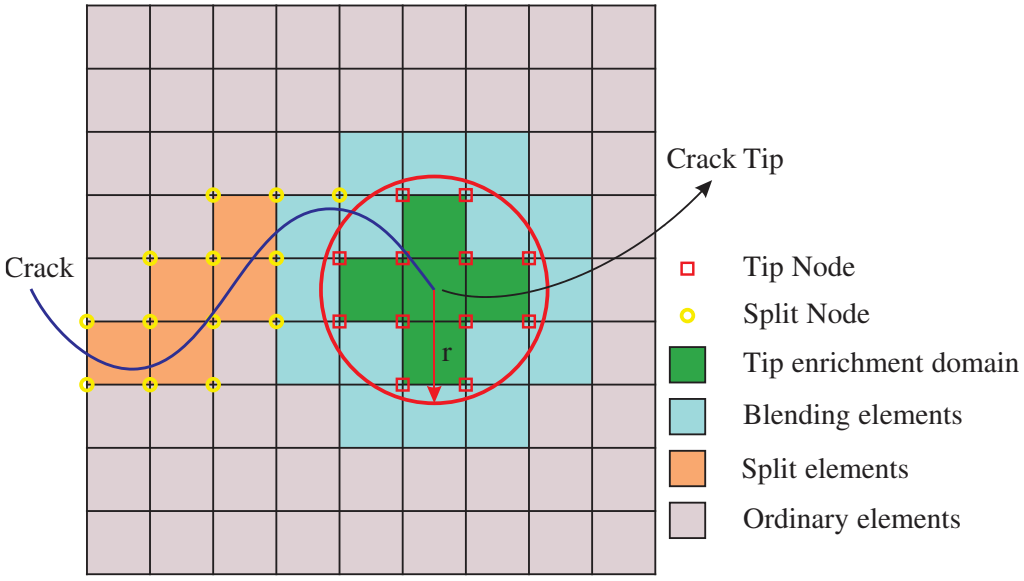

Fig. 2. Description of different elements in XFEM modelling.

3.1. Anisotropic enrichment functions

Asadpoure et al. [16, 46, 47] and Cahill et al. [18] investigated various enrichment functions for orthotropic texture. In general, crack tip enrichment functions in polar coordinates (r,θ) are described as follows [16],

$$F(r,\theta)=\left\{\sqrt{r}\cos\left(\frac{\theta_1}{2}\right)\sqrt{g_1(\theta)},\sqrt{r}\cos\left(\frac{\theta_2}{2}\right)\sqrt{g_2(\theta)},\sqrt{r}\sin\left(\frac{\theta_1}{2}\right)\sqrt{g_1(\theta)},\sqrt{r}\sin\left(\frac{\theta_2}{2}\right)\sqrt{g_2(\theta)}\right\} \quad (11)$$

where θ_1,θ_2,g_1 and g_2 are defined as follows;

$$g_j(\theta)=\sqrt{\left(\cos(\theta)+\alpha_j\sin(\theta)\right)^2+\left(\beta_j\sin(\theta)\right)^2} \quad (j=1,2) \quad (12)$$

$$\theta_k(\theta)=tan^{-1}\left(\frac{\beta_k\sin(\theta)}{\cos(\theta)+\alpha_k\sin(\theta)}\right) \quad (k=1,2) \quad (13)$$

As previously mentioned, the roots of the characteristic equation (Eq. (6)) are in complex form. These roots are in form of $\mu_1=\alpha_1+i\beta_1$ and $\mu_2=\alpha_2+i\beta_2$, where α_k and β_k ($k=1, 2$, see Eqs. 12 and 13) are the real and imaginary parts. According to the study of Bayesteh and Mohammadi [17] the asymptotic crack tip fields can be considered as auxiliary fields for the calculation of SIFs at crack tips in anisotropic materials.

3.2. Calculating stress intensity factors

Mode *I* and *II* SIFs can be calculated by means of interaction integrals. In recent years, Kim and Paulino have introduced various solutions including non-equilibrium, incompatibility, and constant-constitutive-tensor formulations to compute the *J* integral in inhomogeneous materials [87]. Bayesteh and Mohammadi stated that an incompatible formulation is more suitable for *J* integral [17] because this method contains less complicated derivatives while having the same degree of accuracy as a non-equilibrium formulation. Meanwhile, constant-constitutive-tensor results in unacceptable accuracy in finite element formulation [17, 86].

To combine actual and auxiliary fields based on superposition, the *J* integral may be divided into three components: the real (J), auxiliary (J^{aux}) and the interaction (M^l), respectively;

$$J^s=J+J^{aux}+M^l, \quad (14)$$

where J and J^{aux} are related to the actual and auxiliary parts of the J integral, respectively. J^{aux} is defined as follows,

$$J^{aux} = \int_A \left(\sigma_{ij}^{aux} u_{i,1}^{aux} - w^{aux}\delta_{1j}\right) q_{,j} dA + \int_A \left(\sigma_{ij}^{aux} u_{i,1}^{aux} - w^{aux}\delta_{1j}\right)_{,j} q dA \tag{15}$$

where w, is the strain energy density and q is a smooth function which varies from 1 on the interior boundary of A to 0 on the outer one [30]. In Eq. (14) M^l is a local integral which is calculated with the following conversion,

$$M^l = M_1^G \cos(\theta) + M_2^G \sin(\theta) \tag{16}$$

where

$$\begin{aligned} M_m^G &= \int_A \left\{ \sigma_{ij}\, u_{i,m}^{aux} + \sigma_{ij}^{aux} u_{i,m} - \frac{1}{2}\left(\sigma_{ik}\, \varepsilon_{ik}^{aux} + \sigma_{ik}^{aux}\, \varepsilon_{ik}\right)\delta_{mj} \right\} q_{,j}\, dA \\ &+ \int_A \left\{ \sigma_{ij}\left(u_{i,mj}^{aux} - \varepsilon_{ij,m}^{aux}\right) - C_{ijkl,m}\, \varepsilon_{ij}\, \varepsilon_{kl}^{aux} \right\} q\, dA \qquad (m = 1,2) \end{aligned} \tag{17}$$

The equivalent domain integral (A) of Eq. (17) is shown in Fig. 3 where in each arbitrary representative region around the crack tip $C_{ijkl}(r) \neq C_{tip}$ for $r \neq 0$ because of heterogeneity in material properties.

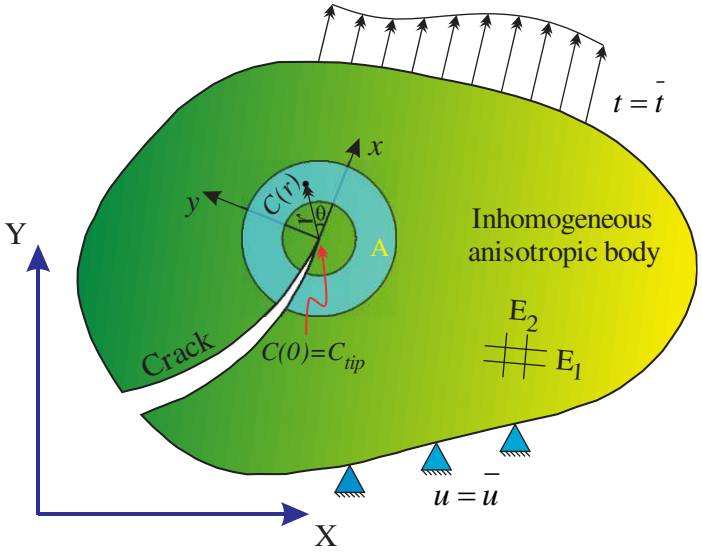

Fig. 3. Equivalent domain integral. Notice that $C(r) \neq C_{tip}$ for $r \neq 0$.

The energy release rate can be described as follows [87],

$$G = J = c_{11} K_I^2 + c_{12} K_I + 2 c_{22} K_{II}^2 \tag{18}$$

in which components c_{ij} are related to the crack tip and can be calculated as follows,

$$c_{11} = -\frac{a_{22}^{tip}}{2} Im\left(\frac{\mu_1^{tip} + \mu_2^{tip}}{\mu_1^{tip}.\mu_2^{tip}}\right) \tag{19}$$

$$c_{12} = -\frac{a_{22}^{tip}}{2} Im\left(\frac{1}{\mu_1^{tip}.\mu_2^{tip}}\right) + \frac{a_{11}^{tip}}{2} Im(\mu_1^{tip}.\mu_2^{tip}) \tag{20}$$

$$c_{22} = \frac{a_{11}^{tip}}{2} Im(\mu_1^{tip} + \mu_2^{tip}) \tag{21}$$

where μ_i^{tip} are the roots of characteristic Eq. (6) and are calculated at the crack tip. Results are simultaneously presented in the simplified equation below by using the superposition of both actual and auxiliary fields in Eq. (18) and replacing $K_{II}^{aux} = 0, K_I^{aux} = 1$ and $K_{II}^{aux} = 1, K_I^{aux} = 0$ [17, 30, 86],

$$\begin{cases} M_1^l = 2c_{11}K_I + c_{12}K_{II} & (K_I^{aux} = 1, K_{II}^{aux} = 0) \\ M_2^l = c_{12}K_I + 2c_{22}K_{II} & (K_I^{aux} = 0, K_{II}^{aux} = 1) \end{cases} \tag{22}$$

These series of equations should be solved to evaluate mode *I* and *II* of SIFs. In inhomogeneous problems, any material properties (we show them with *P* in general), such as elastic modulus E_{11}, E_{22}, shear modulus G_{12}, Poisson ratios v_{12}, v_{21}, vary within the domain in a specified range. If function φ is predefined e.g. from laboratory experiments; then we could have,

$$P(x, y) = \varphi(x, y) \tag{23}$$

A solution to handle local variation in the constitutive tensor is the isoparametric graded finite element method [88]. The different material properties are interpolated using the FEM shape functions as follows [30],

$$P(x, y) = \sum_{i=1}^{m} N_i(x, y)\, \hat{P}_i \tag{24}$$

where $\hat{P}_i$ are nodal desired material properties, N_i are shape functions, and m is the number of nodal points in the element. In the interaction integral of Eq. (17), C_{ijkl}, can be considered the same as the variable mechanical property *P* and their derivatives may be calculated as follows,

$$\begin{aligned} \frac{\partial P(x, y)}{\partial x} &= \sum_{i=1}^{m} \frac{\partial N_i(x, y)}{\partial x}\, \hat{P}_i \\ \frac{\partial P(x, y)}{\partial y} &= \sum_{i=1}^{m} \frac{\partial N_i(x, y)}{\partial y}\, \hat{P}_i \end{aligned} \tag{25}$$

3.3. Crack initiation and propagation criterion

In this study, the maximum circumferential stress presented by Saouma et al. [89] is adapted for crack propagation in anisotropic inhomogeneous materials. This method and other available criteria are tested and validated by Sutula et al. [24-26]. Saouma et al. [89] used the singular values of Eq. (7) in polar form to determine the direction of the maximum circumferential stress σ_θ in anisotropic media. Following the same procedure and by adding the contribution of the T-stress and removing the higher order terms, we obtain the following form for an arbitrary mixed mode,

$$\sigma_\theta(r,\theta) = \frac{K_I}{\sqrt{2\pi r}} Re[A(\mu_1 B_1 - \mu_2 B_2)] + \frac{K_{II}}{\sqrt{2\pi r}} Re[A(B_1 - B_2)] + T sin^2\theta \,, \tag{26}$$

where A and B_i are calculated as follows,

$$A = \frac{1}{\mu_1 - \mu_2}$$
$$B_i = (\mu_i \sin(\theta) + \cos(\theta))^{3/2} \quad (i = 1,2) \tag{27}$$

Thus, crack propagation starts at a position where the following condition is satisfied

$$\frac{\sigma_\theta}{\sigma_\theta^{max}} = \frac{K_I Re\{A(\mu_1 B_1 - \mu_2 B_2)\} + K_{II} Re\{A(B_1 - B_2)\} + T sin^2\theta}{K_{IC}^x cos^2(\theta + w) + K_{IC}^y sin^2(\theta + \omega)} = 1 \tag{28}$$

where K_{IC}^x and K_{IC}^y are the mode-I critical stress intensity factors along x and y directions, respectively, and θ and ω are introduced in Fig. 1b.

4. Verification and validation of the proposed method in an inhomogeneous anisotropic body

To execute the proposed formulation and perform the required calculations, an XFEM-based numerical code was developed using *Matlab* programming language. To verify the validity of the present approach, the developed numerical code was applied to three specimens with different geometrical and mechanical specifications, and simulation results (SIFs, crack initiation angle, and crack propagation trajectory) were compared with those obtained from experimental tests and reported in the literature. Given the simple shape and ease of preparation of disc specimens, the majority of studies on rock failure mechanisms utilize this type of specimen. Therefore, two numerical examples were conducted on common disk shaped specimens in the form of Cracked

Brazilian Disc (CBD) subjected to diametrical compression and Hollow Centre Cracked Disc (HCCD). Considering the lack of any comprehensive rock mechanics study on the failure of inhomogeneous anisotropic materials, one of the numerical models presented in the related literature was selected to investigate such materials. Fig. 4 shows the geometry and boundary conditions of the three selected examples.

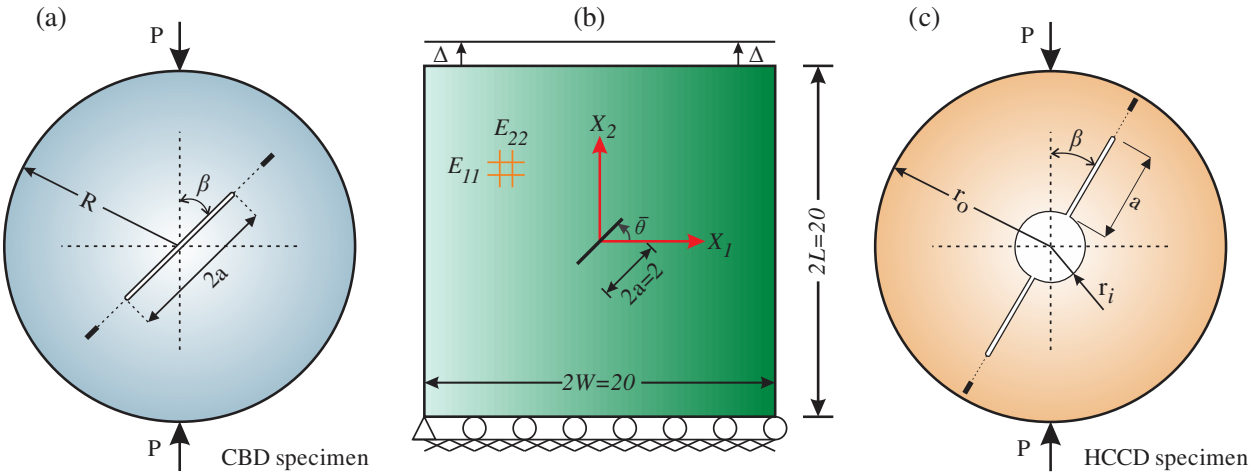

Fig. 4. The geometry and mixed-mode (*I/II*) loading conditions on selected specimens; **(a)** homogeneous anisotropic cracked Brazilian disc; **(b)** inclined center crack in an inhomogeneous anisotropic plate; **(c)** hollow centre cracked inhomogeneous anisotropic disc.

4.1. Mixed-mode fracture in anisotropic homogeneous CBD specimens

Cracked Brazilian Disc (CBD) is one of the rock mechanics specimens commonly used for the study of rock fracture toughness. As shown in Fig. 4a, CBD is a disc of radius R and a crack of length $2a$ at its center. The load P must be applied diagonally on the specimen up to the failure point. In this test, the initial crack angle (β) is defined as the angle between the crack direction and the direction of loading. Depending on the crack angle, the specimen can undergo pure mode *I*, pure mode *II*, or mixed mode *I/II* failure [21].

In a series of studies conducted by Chen et al. [20, 22, 27], the crack initiation angle in homogeneous anisotropic CBD specimens made of marble and shale were investigated both experimentally and numerically with the Boundary Element Method (BEM). Chen et al. [90, 91] proposed the indirect (Brazilian) tensile strength to determine mechanical properties of rock specimens. They also studied the effects of crack length, initial crack angle, and anisotropic orientation on the mixed mode stress intensity factors of a hypothetical anisotropic material using the CBD configuration and BEM analysis. Table 1 shows the obtained crack initiation angles from

the experiments, reported BEM analysis [20], and the proposed XFEM approach for the CBD specimens with *a/R= 0.3*, anisotropic orientation angles of λ*= 0º, 45º, 90º*, and different values of initial crack angle β. As the table shows, the observed results from the XFEM analysis fit well with the other methods. It should be noted that the counterclockwise rotation of the crack with respect to the initial orientation is assumed as positive, and the opposite direction is assumed as negative.

Table 1- Comparing different methods to predict the crack initiation angle for anisotropic CBD specimens

	β (deg.)	Ave. Exp. results (deg.)	Num. results by BEM [20]	Num. results by XFEM
λ = 0°	0	-0.5	0	0
	0	-0.3	0	0
	28.2	74.6	71.87	75.43
	28.2	77.7	71.78	75.59
λ = 45°	0.8	3.0	0.99	3.68
	0.8	5.3	1.06	3.71
	27.6	66.4	70.50	70.09
	27.6	70.7	70.46	70.21
λ = 90°	0	-1.9	0	0
	0	1.0	0	0
	25.9	65.4	69.44	67.01
	25.9	66.6	69.49	67.11

Fig. 5 shows the variation of the normalized mode *I* and *II* of SIFs for different anisotropic orientations of λ, and initial crack angles of β (these parameters are introduced schematically in Fig. 1b). In this example, $E_1/E_2=7$, $E_1/G=3$, *a/R=0.5*, *v=0.25*, and the normalized mode *I* and *II* of SIFs are as follows;

$$Normalized\ Mode\ I\ of\ SIF = \frac{K_I}{K_0}, \quad Normalized\ Mode\ II\ of\ SIF = \frac{K_{II}}{K_0}, \quad K_0 = \frac{p}{\pi R t}\sqrt{\pi a}$$

Fig. 4a provides the descriptions of all the above-mentioned parameters for the CBD specimen. According to Fig. 5, the SIFs are considerably influenced by not only the initial crack angle β, but also the material orientation angle λ. For example, at β*=0º*, variation of λ from 0º to 90º causes to change the normalized K_I up to -61.6%. While at β*=38º*, with increasing the value of λ from 0º to 90º, the maximum fluctuation in the absolute value of the normalized K_{II} is +75.2%. Given such an effect, the simplification of anisotropic materials by assuming isotropy will result in unrealistic solutions. When the material orientation angle λ is fixed and the crack is parallel to the loading direction (i.e. β *= 0º*), the mode *I* of SIF becomes positive and reached maximum value. When the crack is perpendicular to the loading direction (i.e. β *= 90º*), this factor shows a minimum negative value. When the crack angle β, is 0º and 90º, the mode *II* stress intensity factor is negligible, and the maximum absolute value is achieved about β = 40º. Pure mode *II* occurs when

$K_I = 0$. According to Fig. 5a, this angle significantly depends on the orientation of the anisotropy axes. Thus, suggesting a constant initial crack angle for all cases is not justified. For the elastic ratios assumed in this example, this angle varies from 15° to 42° depending on the value of λ. In general, the SIFs are significantly dependent not only on β, but also on λ.

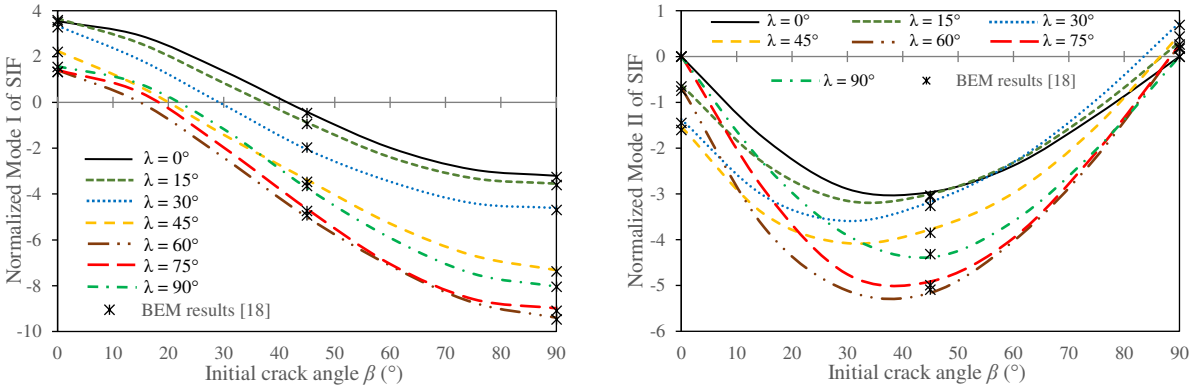

(a) (b)

Fig. 5. Variation of normalized mode *I* **(a)**; and *II* **(b)**, stress intensity factors for different values of anisotropic orientation angle λ, and initial crack angle β.

4.2. Inhomogeneous (isotropic and anisotropic) plate with an inclined center crack

Consider, as shown in Fig. 4b, an inhomogeneous plate subjected to plane stress and experiencing a uniform strain $\bar{\varepsilon}$ that corresponds to an uncracked structure. The plate has a crack length of a at angle $\bar{\theta}$ (counter-clockwise) subjected to fixed-grip loading. Two states are considered for the plate: *i*) inhomogeneous and isotropic and *ii*) inhomogeneous and anisotropic. For the former state we have $\sigma_{22}(X_1, 10) = \bar{\varepsilon}E^0 e^{\alpha X_1}$, and for the later, we have $\sigma_{22}(X_1, 10) = \bar{\varepsilon}E_2^0 e^{\alpha X_1}$. Young's modulus and shear modulus are exponential functions of X_1, the Poisson ratio is constant, and geometric parameters are as follows;

$$\alpha = 0.5\,, \qquad a/W = 0.1\,, \qquad L/W = 1.0\,, \qquad \bar{\theta} = 0 - 90\,, \qquad \bar{\varepsilon} = 1 \tag{29}$$

where in the inhomogeneous isotropic case;

$$E(X_1) = E^0 e^{\alpha X_1}\,, \qquad \nu(X_1) = \nu$$
$$E^0 = 1.0\,, \qquad \nu = 0.3 \tag{30}$$

and in the inhomogeneous anisotropic case;

$$E_1(X_1) = E_1^0 e^{\alpha X_1}\,, \quad E_2(X_1) = E_2^0 e^{\alpha X_1}\,, \quad G_{12}(X_1) = G_{12}^0 e^{\alpha X_1}\,, \quad \nu_{12}(X_1) = \nu_{12}^0$$
$$E_1^0 = 10^4\,, \qquad E_2^0 = 10^3\,, \qquad G_{12}^0 = 1216\,, \qquad \nu_{12}^0 = 0.3 \tag{31}$$

The isotropic case was previously studied by Konda and Erdogan [92] with semi-analytical solutions, Dolbow and Gosz [45] with the XFEM approach, and Kim and Paulino [87] by singular finite element method. The anisotropic case was also studied by Kim and Paulino [87] assuming non-equilibrium and incompatibility formulations of the *M* integral.

To simulate this example by the proposed method, approximately 2944 degrees of freedom were used (1396 four-node elements), while it was solved by Kim and Paulino [87] with the singular finite element method and 10672 degrees of freedom (5336 elements). Table 2 shows the normalized SIFs of both the inhomogeneous isotropic and inhomogeneous anisotropic cases for the present method and the reported results in the literature, where *R* and *L* superscripts indicate the SIFs at the right and left crack tips, respectively. Clearly good agreement is observed between the present method and reference results.

Table 2- Comparison of normalized mixed-mode SIFs in isotropic ($K_0 = \bar{\varepsilon}E^0\sqrt{\pi a}$) and anisotropic ($K_0 = \bar{\varepsilon}E_2^0\sqrt{\pi a}$) inhomogeneous cases.

Isotropic case					
Method	$\bar{\theta}$	K_I^R/K_0	K_{II}^R/K_0	K_I^L/K_0	K_{II}^L/K_0
Konda and Erdogan [86]	0°	1.424	0.000	0.674	0.000
	36°	0.925	0.548	0.460	0.365
	72°	0.146	0.314	0.059	0.269
Nonequilibrium formulations of the *M* integral [81]	0°	1.4234	0.0000	0.6657	0.0000
	36°	0.9224	0.5502	0.4559	0.3625
	72°	0.1451	0.3147	0.0587	0.2670
Constant-constitutive tensor formulations of the *M* integral [81]	0°	1.4262	0.0000	0.6629	0.0000
	36°	0.9224	0.5512	0.4546	0.3607
	72°	0.1439	0.3144	0.0596	0.2670
Dolbow and Gosz (XFEM) [45]	0°	1.445	0.000	0.681	0.000
	36°	0.930	0.560	0.467	0.364
	72°	0.142	0.316	0.062	0.268
Presented XFEM formulations	0°	1.4291	-0.0000	0.6683	0.0002
	36°	0.9231	0.5557	0.4570	0.3598
	72°	0.1400	0.3215	0.0658	0.2583
Anisotropic case					
Method	$\bar{\theta}$	K_I^R/K_0	K_{II}^R/K_0	K_I^L/K_0	K_{II}^L/K_0
Nonequilibrium formulations of the *M* integral [81]	0°	1.4279	0.0000	0.6663	0.0000
	36°	1.0177	0.4097	0.4150	0.4160
	72°	0.2154	0.2906	0.0056	0.2822
Incompatiblity formulations of the *M* integral [81]	0°	1.4285	0.0000	0.6663	0.0000
	36°	1.0177	0.4111	0.4149	0.4156
	72°	0.2158	0.2906	0.0052	0.2823
Presented XFEM formulations	0°	1.4294	0.0000	0.6601	0.0000
	36°	1.0097	0.4132	0.4083	0.4180
	72°	0.2178	0.3017	0.0059	0.2792

The first mode of normalized stress intensity factors at the right crack tip in the case of $\bar{\theta} = 0$ is considered to investigate convergence of error of normalized SIFs. Fig. 6 shows the convergence rate of results for both isotropic and anisotropic cases. In isotropic case, results are compared with semi-analytical solution by Konda and Erdogan [92]. Since there is no available exact solution for anisotropic case in the literature, the average value of normalized stress intensity factors which are obtained by Nonequilibrium and incompatible formulations of the *M* integral by Kim and Paulino [87], has been considered as the exact value. In both cases, a good convergence rate is observed.

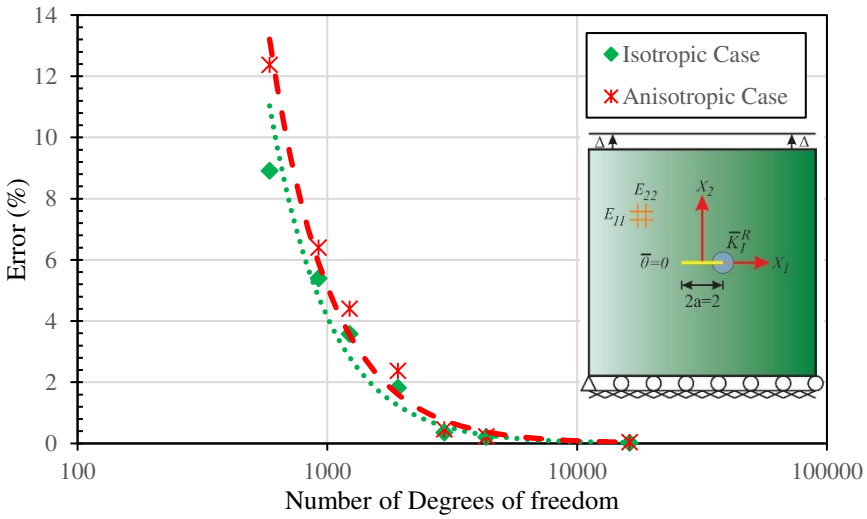

Fig. 6. Semi-logarithmic graph for convergence rate of normalized K_I at the right crack tip in the case of $\bar{\theta} = 0$ for both isotropic and anisotropic cases.

4.3. Inhomogeneous anisotropic Hollow Centre Cracked Disc

To gauge the strength of the proposed method in simulating the failure mechanism of inhomogeneous anisotropic rocks, it needs to be validated for such materials. According to Mohtarami et al. [9], when a porous rock material is exposed to a corrosive acidic fluid, the *pH* and concentration of the chemical solution and thus its corrosiveness decrease as it penetrates into the rock. This behavior diminishes mechanical properties of the points in the vicinity of the chemical source [93]. In other words, the mechanical properties of rocks will be functions of time and distance to the location of the acid source. Mohtarami et al. [4, 94] utilized this observation to simulate the effect of different parameters on the efficiency of oil wells acidizing. They found that the degree of variations and the type of rock inhomogeneity depend on the parameters such as temperature, acid injection pressure, acid-rock contact time, confining pressure, concentration and type of acidic fluid, and the type of rock. Based on this concept, the device shown in Fig. 7 was

designed and constructed to create inhomogeneous and anisotropic specimens by injecting acid to the permeable porous rock material. The device is able to inject acidic fluid with a specific pressure or flow rate, apply confining pressure and heat, and then measure the parameters of the outflow. It consists of a 4 cm thick hollow stainless steel cylinder capable of sustaining confining stress and acid pressures of up to 30 MPa and temperatures up to 200ºC. Also according to Fig. 8, cylindrical rock specimens with an outer diameter of 123 mm and height of 180 mm and with a central hollow with diameter of 20 mm and depth of 150 mm were prepared. The device has an internal cap that, once mounted on the specimen, drives the acid path in a way that it enters in and contacts only with the exposed surface within the central hole. This would result in acid penetration into the specimen as radially as possible.

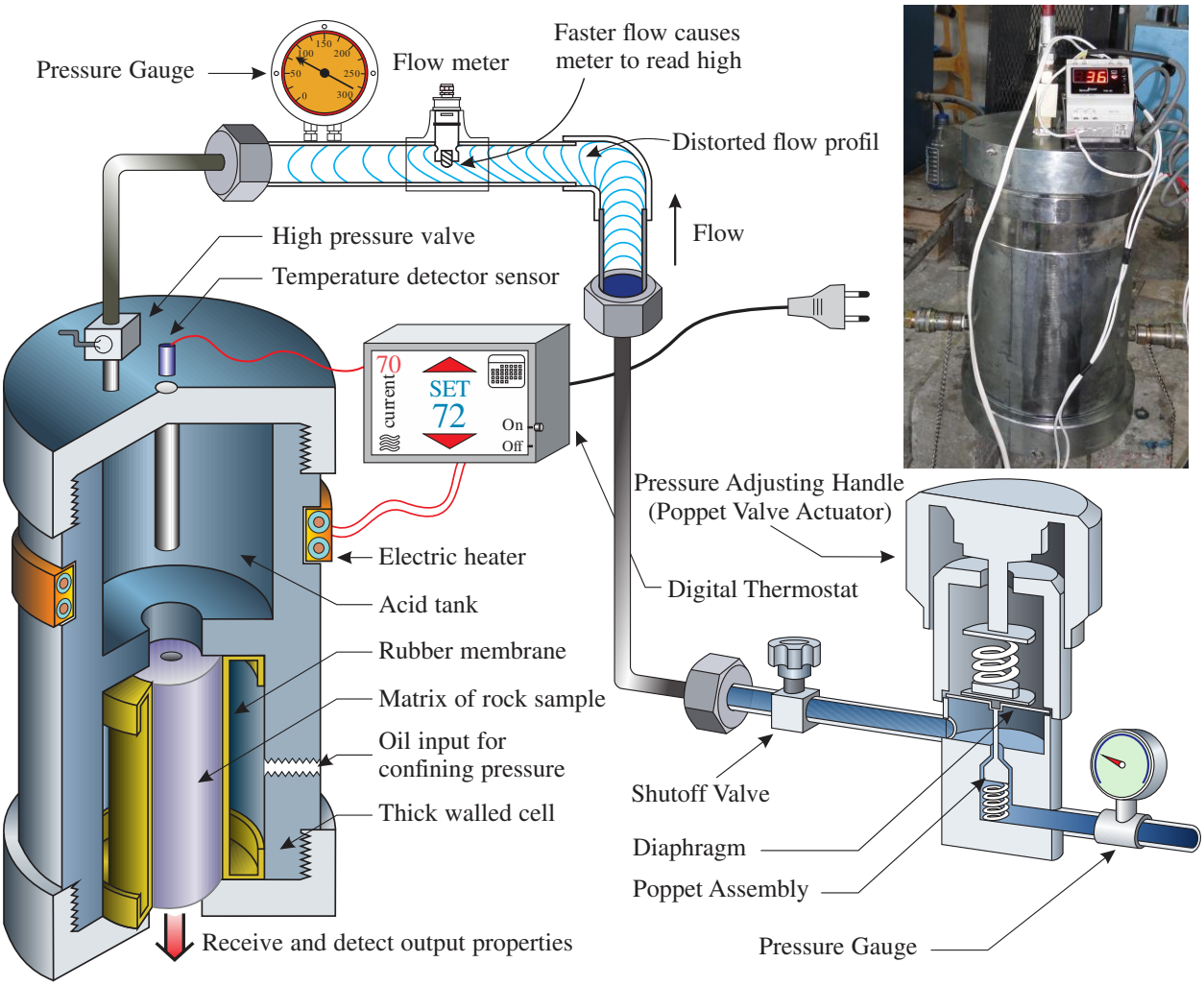

Fig. 7. Schematic and real view of designed device to simulate the acidizing process.

Fig. 8. Prepared cylindrical specimens for acidizing tests (external diameter 123 mm, inner diameter 20mm, length 180 mm).

The specimens were extracted from a rock body belonging to Asmari formation in Iran. The major mineral composition of this formation is calcite and dolomite (totally 86%) with a small portion of siderite and other minerals. All samples were obtained from the same location and with the minimum distance from each other. Samples were also subjected to a series of ultrasonic tests to identify the most similar samples for the ensuing tests. Fig. 9 compares the produced images by a scanning electron microscope (SEM) with a magnification of 500, in sound sample and acidized sample with 15% *HCl* at 60ºC. As evident, the porosity of the sample has increased by acidizing. Fig. 10 also shows the locus of pores in two orthogonal directions with respect to distance from the acid source in the same rock specimen. It can be seen that, zones near the central hollow exhibit a higher value of porosity. This means that acidizing creates an inhomogeneous environment where points closer to the chemical source exhibit more reduced mechanical properties. The increasing rates of porosity along two orthogonal directions are dissimilar. The reason for this dissimilarity is the presence of weakness planes (joint sets and fractures), which facilitate the penetration of acid along a particular direction (parallel to the weakness plane). This phenomenon shows that acidizing creates an anisotropic environment.

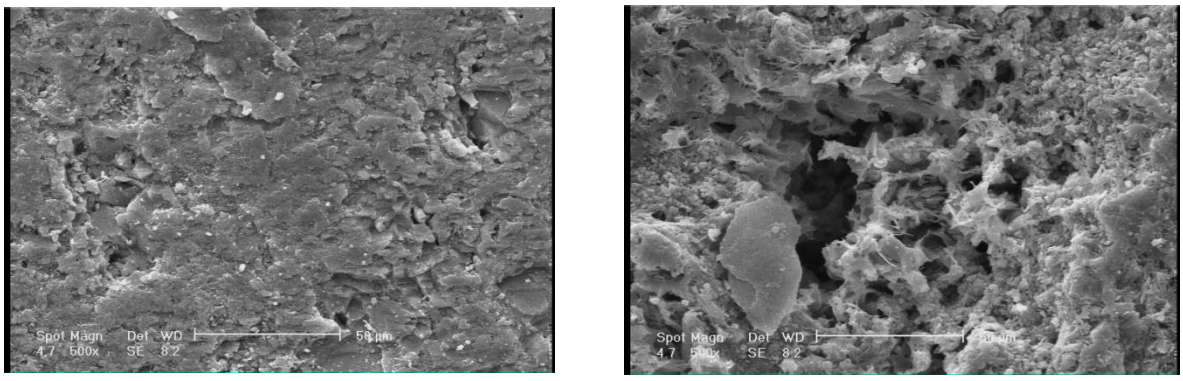

(a) (b)

Fig. 9. Images of a SEM with magnification of 500 for: **a)** a sound sample; **b)** an acidized sample with 15% HCl at 60ºC.

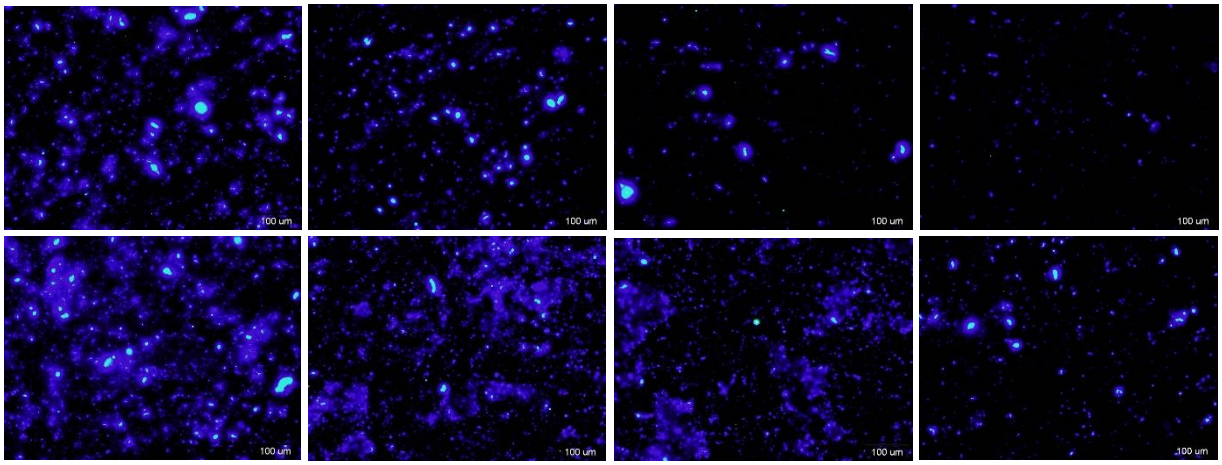

Fig. 10. Increasing porosity (bright spots) in two orthogonal directions in acidizing by 15% HCl at 60ºC. Left to right in distance of 5, 20, 35, 45 mm from acid contact point; photos by a fluorescent microscope and 40× magnification.

Determining mechanical properties at a desired point of the rock material requires access to the mechanical properties of the rock matrix, the porosity percentage, and the shape of the pores in that point. The properties of a porous material largely depend on the extent of porosity as well as internal pore structure, so that several models have been developed specifically to predict the structure-dependent mechanical performance of porous materials [95-97]. The Mori-Tanaka (MT) model [98, 99] is one of the best-known analytical solutions for determining the effective constants of porous and composite materials by the use of homogenization techniques. In this method, the Eshelby tensor is determined by the use of Eshelby's equivalent inclusion theory [100] and then the homogenization technique is utilized to determine the properties of porous materials. Gang et al. [101] have resolved the limitations of the Mori-Tanaka model by the use of a stepped equivalent substitution (SES) approach to calculate the elastic constants of porous materials with different amounts of pores of different sizes.

Consider a material containing ellipsoid pores subjected to a uniform stress σ^0. An inhomogeneous material that contains inclusions (or pores) is an Eshelby's inhomogeneous inclusion problem, so the equivalent stiffness matrix of the porous solid (L^e) will be as follows,

$$L^e = L^m(I + \phi A)^{-1} \tag{32}$$

where L^m is the stiffness matrix of the matrix material, I is the fourth rank identity tensor, ϕ is the volume fraction of the pores (i.e. porosity), and

$$A = \{L^m - L^m[\phi I + (1-\phi)S]\}^{-1} L^m \tag{33}$$

where S is the Eshelby's tensor for pores [99]. In the extended Mori-Tanaka (EX-MT) approach, when a matrix contains multiple groups of pores with different shapes, sizes and directions, the MT model must be used to turn the matrix and the first group of pores into an equivalent material with stiffness matrix L^1. This equivalent material is considered as a new matrix which makes a porous material with the remaining pores. Reusing the MT model with the second pore group gives another equivalent material with stiffness matrix L^2. By repeating this process, the interaction between all pores can be analyzed and a final equivalent material (with the stiffness matrix of L^e) will be obtained. Hence, the equivalent flexibility matrix will ultimately be equal to $\mu^e = (L^e)^{-1}$. The effective transverse elastic modulus ($E_{\parallel}$) and the effective longitudinal elastic modulus ($E_{\perp}$) of the porous material can be obtained as follows [101];

$$E_{\parallel} = (\mu_{11}^{e})^{-1}, \qquad E_{\perp} = (\mu_{33}^{e})^{-1}. \tag{34}$$

This method has been validated in compound materials [102], metal alloys [103], composites [104], and recently in concrete [105], brittle [106, 107] and quasi-brittle [108] rocks. Having the shape and distribution of porosity and the properties of rock matrix, the mechanical properties of any desired point of the object can be easily determined. Fig. 11 shows the distribution of elastic moduli obtained by the use of extended Mori-Tanaka method for a specimen after 24 hours of acidizing with 15% *HCl* and injection pressure of 4 MPa. As can be clearly observed, this method allows the mechanical properties of any desired point to be determined.

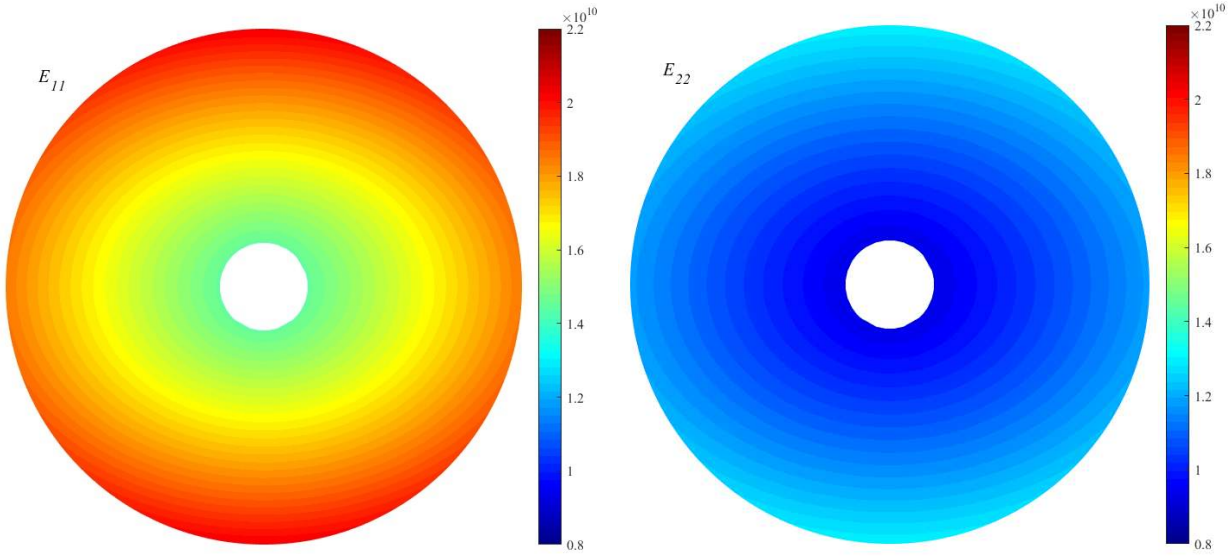

(a) (b)

Fig. 11. Distribution of elastic modulus (unit: *Pa*) in tested HCCD specimens in a similar scale, **a)** distribution of E_{11}; **b)** distribution of E_{22}.

After initial preparations and acidizing process, the cylindrical specimens were cut at *t=30* mm intervals along the cylinder axis to obtain disc-shaped specimens. Two straight cracks (according to HCCD sample in Fig. 4c) were then created in the disc specimens at different initial angles (β) such that $a/(r_o-r_i)=0.2$ and $r_o=123$ mm, using a wire saw. The specimens were placed between the steel jaws of testing machine as suggested by ISRM [109], and were subjected to a linear load at a slow deformation rate of 0.5 mm/min until failure. The ultimate loads and crack propagation trajectory of all the specimens were recorded. Table 3 shows the geometric characteristics of the selected specimens, and Fig. 12 also presents a view of these tested HCCD specimens after failure. Secondary cracks which are formed after the main crack, were mostly located along the weakness planes due to the fact that the loading does not stop immediately. Non-original cracks propagation because of reasons such as absence of momentary interruption in loading and the effects of boundary conditions has already been reported for rocks in the literature [14, 19, 23, 91]. In all of these specimens, cracks showed a tendency to propagate toward the loading point.

Table 3- The geometric characteristics of the selected HCCD specimens for comparison of experimental and numerical results

Sample's Fig. No.	β (Deg)	λ (Deg)	r_o (*mm*)	r_i / r_o	$a / r_o - r_i$	t (*mm*)
Fig. 12a	0	0	163	0.20	0.2	29.9
Fig. 12b	15	60	163	0.18	0.2	30.2
Fig. 12c	28	90	163	0.22	0.2	30.0

(a) (b) (c)

Fig.12. Selected HCCD specimens after failure; **a)** pure mode I; **b)** mixed mode I/II; **c)** pure mode II.

In Fig. 13, the experimental crack propagation path is compared with the trajectory predicted by the XFEM. This figure demonstrates the excellent ability of the proposed method to predict crack trajectory in inhomogeneous anisotropic materials. Fig. 14 shows the distribution of stresses

in the three selected samples. Examination of the stress distribution shows that whenever the crack deviates from the vertical position or anisotropic axes deviate from 0º or 90º, the induced stresses become asymmetric. In addition, a closer examination of shear stresses and σ_{xx} applied to the crack surfaces shows that as a crack deviates from the pure mode *I* ($\beta = 0°$) to the pure mode *II* ($\beta = 28°$), the shear stresses within this region increase substantially. This suggests an increase in the contribution of the sliding mode on sample fracturing. On the other hand, tensile stresses acting on the crack surfaces decrease (reduction of tensile mode) and instead, the maximum tensile stresses become concentrated at the top of the central hollow. With further increase in the initial crack angle and in the presence of sufficient diagonal force, this point of the body becomes susceptible to nucleation and propagation of a new crack.

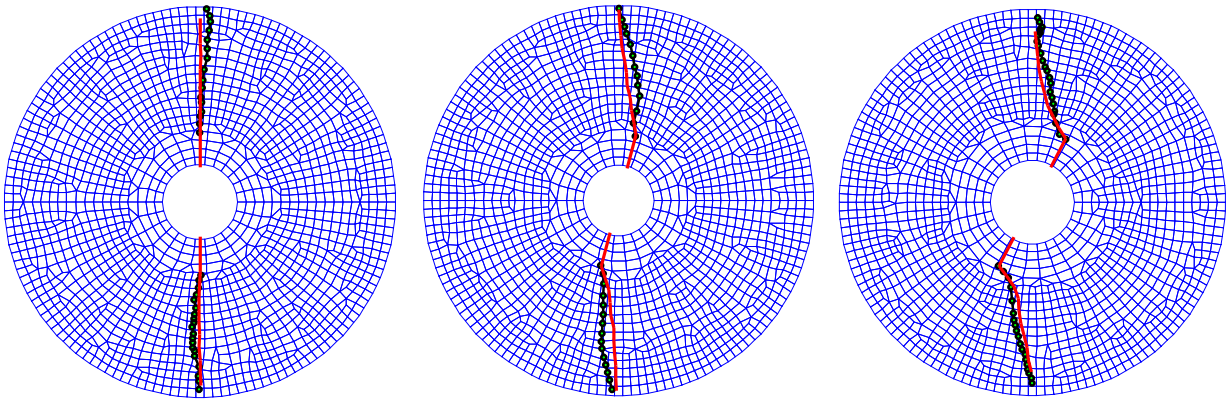

Fig. 13. Comparison of crack propagation trajectory obtained by numerical method (continuous line) and experimental method (line with solid circles) respectively for: **a)** pure mode I; **b)** mixed mode I/II; **c)** pure mode II.

5. Effect of geometrical and mechanical properties on SIFs in the HCCD specimen

As previously mentioned, the assumptions of isotropy and homogeneity cannot account for actual conditions in rock formations and furthermore, there is no comprehensive rock mechanics test for investigating the toughness of inhomogeneous anisotropic geo-materials. Therefore, in this section, we conduct a parametric study on the geometric and mechanical properties of such materials by the use of a HCCD configuration. The reason for choosing this particular specimen and test configuration was the ease of specimen preparation, the simplicity of the test procedure and apparatus operation, and the fact that this is the only option for high-pressure acid injection. This test has already been successfully used for homogeneous isotropic [110] and homogeneous anisotropic rocks [19]. Since previous studies [17, 27, 87] have shown the insignificant effect of Poisson's ratio on SIFs and failure parameters, in all analyses, this ratio was assumed to be

constant. According to Bayesteh and Mohammadi [17] and Kim and Paulino [87], in inhomogeneous materials, the degree of anisotropy (E_1/E_2), material orientation angle (λ), and magnitude of variation pattern (α) have significant effects on determination of SIFs. Chen et al. [19, 20] have studied the impact of varying E_1/E_2 within the range of $^1/_7$ - 7 on SIFs of anisotropic homogeneous cracked Brazilian disks. In the present study, the same values of degree of material anisotropy were considered for HCCD test of anisotropic inhomogeneous material. The material orientation angle (λ) can vary in the range of 0°-90°, so this study was conducted with four orientation angles of λ=0,30,60, and 90. Concurring with the study of Chen et al. [20] on the effect of shear modulus in homogeneous materials, five ratios of E_1/G = 0.25, 0.5, 1, 2, and 4 were selected. Finally, to study the effect of inhomogeneity, the rate of varying mechanical properties (α) (see Sec. 4.2 and Eqs. 30-31) was changed in the range of -10 to +10 and the resulting effects were examined. Assuming exponential changes in mechanical properties, the numbers in the aforementioned range provide reasonable elastic moduli. Sensitivity analysis was conducted on the degree of anisotropy (E_1/E_2), orientation angle (λ), shear stiffness (G), and the rate of inhomogeneity (α) as mechanical parameters, and the initial crack length (a), and its angle (β) as geometrical parameters. But before discussing the results, the following definitions need to be outlined.

Normalized Stress intensity factors (NSIFs): This ratio is defined for Modes *I* and *II* as follows,

$$\overline{K_I} = \frac{K_I}{K_0}, \qquad \overline{K_{II}} = \frac{K_{II}}{K_0}$$

where, for a sample with thickness t and radius R, the specified factor is $K_0 = P\sqrt{\pi a}/(\pi R t)$.

Pure mode *I* and pure mode *II*: Typically, loads are a mixture of Modes *I* and *II*. In the HCCD test, specimens may undergo different conditions depending on the crack angle β. The β angle at which $\overline{K_{II}} = 0$ is called the pure mode *I* angle (β_I), and its corresponding $\overline{K_I}$ is called the pure mode *I* normalized stress intensity factor (pure mode *I* NSIF). In this case, there is no sliding mode, and the sample experiences only the tensile mode. Conversely, the β angle at which $\overline{K_I} = 0$ is called the pure mode *II* angle (β_{II}), and its corresponding $\overline{K_{II}}$ is called the pure mode *II* normalized stress intensity factor (pure mode *II* NSIF).

Signs: The sign of $\overline{K_I}$ refers to the relative normal displacement of the crack surfaces, so a positive $\overline{K_I}$ represents an opening crack and a negative $\overline{K_I}$ represents a closing one. While the sign of $\overline{K_{II}}$

refers to the sliding displacement of the crack surfaces relative to each other, a positive $\overline{K_{II}}$ denotes a clockwise sliding and a negative $\overline{K_{II}}$ denotes a counterclockwise one.

Crack length ratio: The dimensionless ratio of $a/(r_o-r_i)$ (see Fig. 4c) is called crack length ratio.

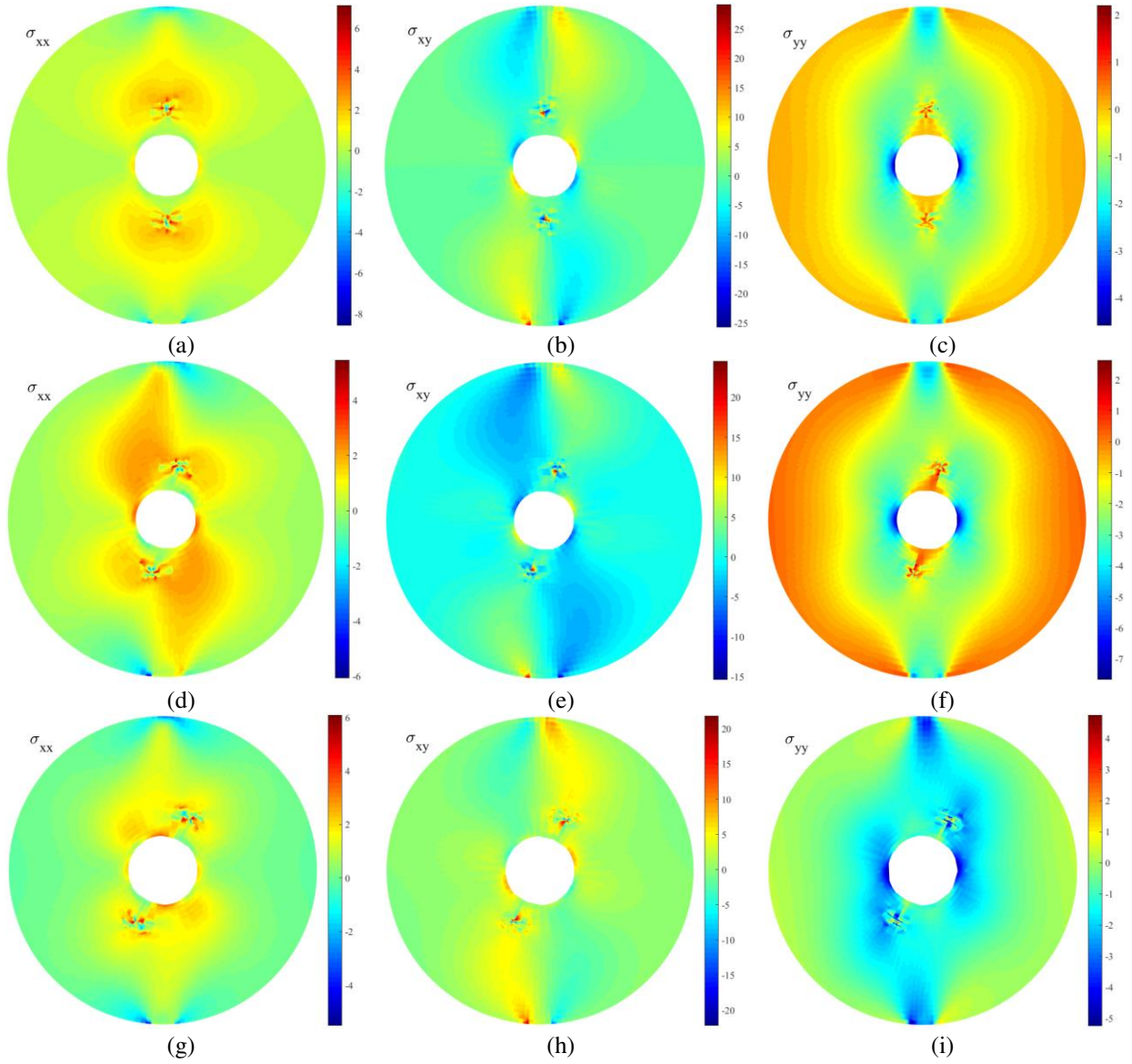

Fig. 14. Distributions of stresses (unit: *MPa*) in HCCD specimens; **a, b, c)** for sample 12*a*; **d, e, f)** for sample 12*b*; **g, h, i)** for sample 12*c*.

5.1. Degree of material anisotropy

The effect of material anisotropy (E_1/E_2) on the values of SIFs, with three different degrees of anisotropy E_1/E_2=$^1/_7$, 1 (isotropic), and 7 are conducted numerically. The material orientation angle and Poisson's ratio are selected as λ = 0 and ν = 0.23, respectively. The dimensionless

geometric parameters are also selected to be the same as the setup of laboratory experiments, and are $a/(r_o-r_i)=0.2$ and $r_i/r_o=0.17$. Fig. 15 represents the effect of different degrees of anisotropy on the NSIFs for various initial crack angles (β). As it can be clearly seen, the NSIFs of the first fracture mode $\overline{K_I}$ decrease substantially with the increase in the initial crack angle (β), while the NSIFs of the second mode $\overline{K_{II}}$ increase. This trend indicates SIFs dependency to the crack angle. The observed trend in this example is also found in the study of all other parameters. It is seen that with increasing E_1/E_2; the angle of pure mode *II* (β_{II}) increases from 25º to 37º, the NSIF of pure mode *I* (where $\overline{K_{II}} = 0$) decreases by about 15% and the NSIF of the pure mode *II* (where $\overline{K_I} = 0$) increases by about 18%.

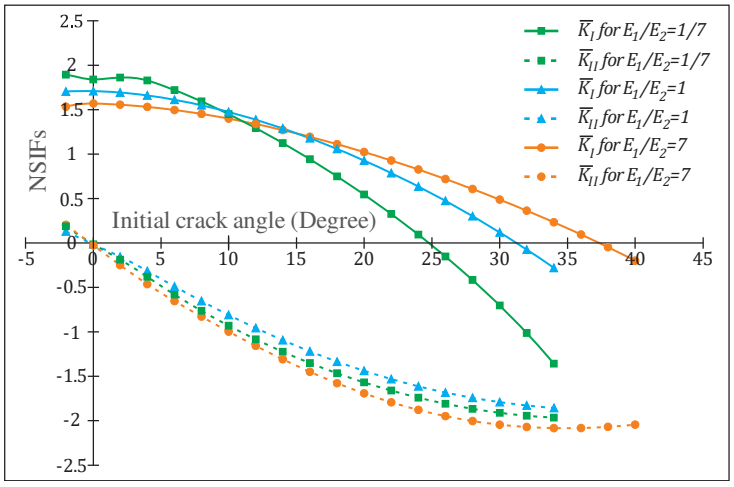

Fig. 15. Variation of normalized SIFs versus the crack initiation angle β, for different degrees of material anisotropy.

5.2. Anisotropic orientation

Numerical analysis of the effect of anisotropy orientation (λ) on SIFs of inhomogeneous anisotropic material was carried out at anisotropy degrees of E_1/E_2=1.5 and 7. For a better comparison, the results of the isotropic specimen (E_1/E_2=1) were also examined. The anisotropy orientation was set to $\lambda=0, 30, 60, 90$ and the rest of the variables were set to the same values as in the example 5.1. Figs. 16a and 16b show the variations of NSIFs for anisotropy orientation of 1.5 and 7, respectively. A closer examination of these figures shows that:

- In both graphs, for material orientation angle $\lambda=0, 90$, pure mode *I* occurs when $\beta=0$. This state is diverted for other values of λ (60 and 30), and the deviation increases with the increase in the degree of anisotropy (chart b).
- Comparing the NSIFs of two charts at the same λ indicates that as E_1/E_2 increases from 1.5

to 7, the greatest change in $\overline{K_I}$ NSIFs graph is related to λ=*90* (+10% variation) while the greatest change in $\overline{K_{II}}$ NSIFs curve is related to λ = 60 (-16.6% variation).

- Although for small anisotropy degrees (Fig. 16a) a change in material orientation angle triggers a small variation in pure normalized mode *I* and *II* SIFs, for large anisotropy degrees (Fig. 16b) the resulting variations are more significant.
- For small anisotropy degrees (E_1/E_2=*1.5*), when λ changes from 0º to 90º, the degree at which pure mode *II* occurs, decreases from about 34º to 26º while for large anisotropy degrees (E_1/E_2=*7*), the reduction is from 38° to about 20°.

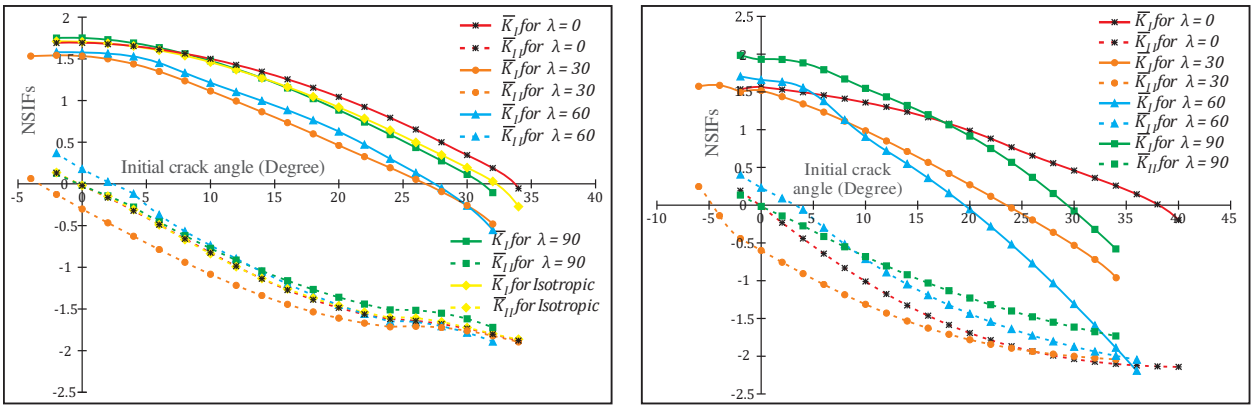

(a) (b)

Fig. 16. Normalized SIFs versus the crack initiation angle β, for different material orientation angle; **a)** for isotropic case and anisotropy degree of 1.5; **b)** anisotropy degree of 7.

5.3. Shear modulus

The effect of shear stiffness on NSIF was investigated when E_1/E_2=*1.5*, λ=*0*, and for a constant value of E_1 but variable ratio of E_1/G. The rest of the parameters were set to the same values as in example 5.1. Fig. 17 shows the effect of changes in shear modulus *G* on NSIFs. It is clearly observed that the decrease in *G* (increase in E_1/G) has caused a 9% reduction in the pure mode *I* NSIF ($\overline{K_I}$) and has reduced β_{II} from about 38º to 31º. However, this reduction rate is more significant (18.4%) in the pure mode *II* NSIF ($\overline{K_{II}}$). This observation shows that shear modulus has a greater effect on the pure mode *II* mechanism (shear mode) compared to the other failure mode.

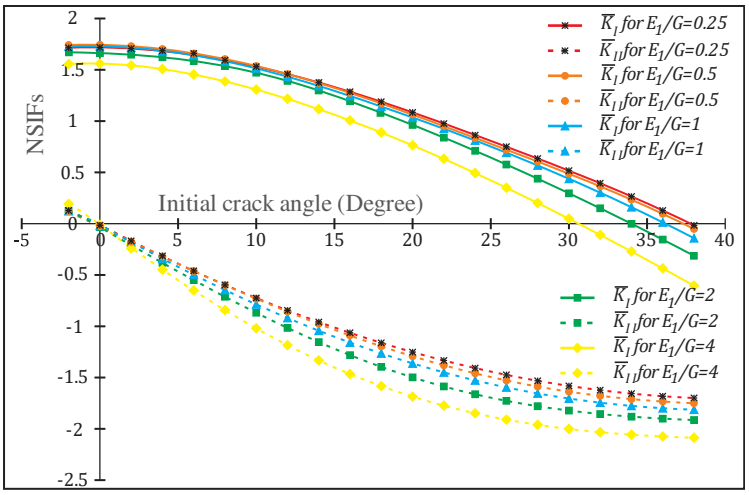

Fig. 17. NSIFs versus the crack initiation angle β, for different shear modules.

5.4. Inhomogeneity order

Similar to the numerical example of Section 4.2, we assume that mechanical properties of the object change exponentially by the equation $\xi = \xi_0 e^{\alpha R}$, where ξ is the desired mechanical property (E_1, E_2, G_{12}) at the desired point, ξ_0 is the mechanical property at the center of the object, e is the Napier number, α is the inhomogeneity order, and R is the distance from the center of the specimen. For this particular example, $E_1^0/E_2^0=1.5$, and the rest of the variables were set to the same values as in the first example, except that the simulated model was not only anisotropic but also inhomogeneous. The inhomogeneity order (α) varied from -10 to +10. Negative α values cause the structure to exhibit weaker properties at its outer layers than its center and positive α values cause the opposite effect. Meanwhile, the greater absolute values of α results in sharper changes in the mechanical properties. Fig. 18 shows the effect of the inhomogeneity order on the values of $\overline{K_I}$ and $\overline{K_{II}}$ for different β values. In this numerical experiment, we can conclude that:

- For mode *I* NSIFs variations do not follow a uniform trend with the inhomogeneity order. For crack initiation angles β of -5° to 15° in particular, there is a negative correlation between α and the absolute value of NSIF (mode *I*) whereas for bigger β values, this correlation is positive. Also, the slope of the variations is not uniform and increases more significantly once the orientation angle is beyond 15°.
- For mode *II* NSIFs, the absolute values of SIF decrease with an increase in the inhomogeneity order. These variations become sharper as β deviates from the pure mode *I* ($\beta = 0$) toward pure mode *II*.

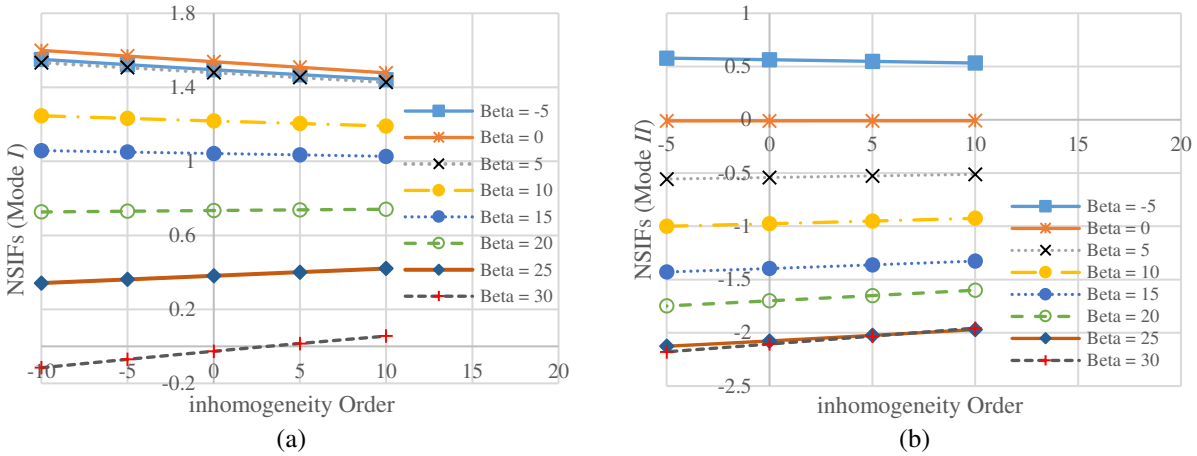

Fig. 18. NSIFs versus variation of inhomogeneity order (α) for different crack initiation angles; **a)** mode *I* of failure; **b)** mode *II* of failure.

5.5. Effect of initial crack length in homogeneous/inhomogeneous anisotropic materials

The effect of initial crack length was investigated by considering cracks of different length ratios $a/(r_o-r_i)$ in homogeneous and inhomogeneous anisotropic HCCD specimens. This was done to examine not only the effect of geometric parameters but also the effect of inhomogeneity on the NSIF results. In this part of the work, the homogeneous material was modeled with $E_1/E_2=3$ and $a/(r_o-r_i)=0.2,0.4,0.6$ and the inhomogeneous material was modeled with $E_1^0/E_2^0=3$, $a/(r_o-r_i)=0.2,0.4,0.6$ and $\alpha=10$. Fig. 19 shows the effect of initial crack length on the two aforementioned materials. Individual investigation of Fig. 19a or 19b shows that the increase in crack length has increased the pure mode *I* and *II* NSIFs by about 25% and 28%, respectively. This increase is far higher in $\overline{K_{II}}$. Conversely, this increase has reduced the angle of pure mode *II* (β_{II}) from about 30º to about 22º. On the other hand, a comparison of these two charts shows that inhomogeneity order has caused a slight change in NSIFs. More specifically, in the homogeneous material, the minimum and maximum $\overline{K_I}$ values at $\beta=0$ are respectively 1.345 and 1.686 but in the inhomogeneous material, these values are 1.301 and 1.737, respectively. Meanwhile, the minimum and maximum $\overline{K_{II}}$ are respectively -2.293 and -2.860 in the homogeneous material and -2.117 and -2.819 in the inhomogeneous material. Also, inhomogeneity has increased the angle of pure mode *II* by approximately 1 to 2 degrees.

It should be noted that even insignificant variations in SIFs do not mean that inhomogeneity can be ignored, as it may disrupt the stress distribution and material deformation and the stiffer part will receive a larger contribution of the applied external force. Also, as suggested by Saouma

et al. [89] and Mohtarami et al. [9], inhomogeneity changes the material's toughness by altering its mechanical properties. Therefore, the required fracture force in an inhomogeneous body is usually not the same as a homogeneous one and it is a function of the mechanical properties of the point where the crack tip is located.

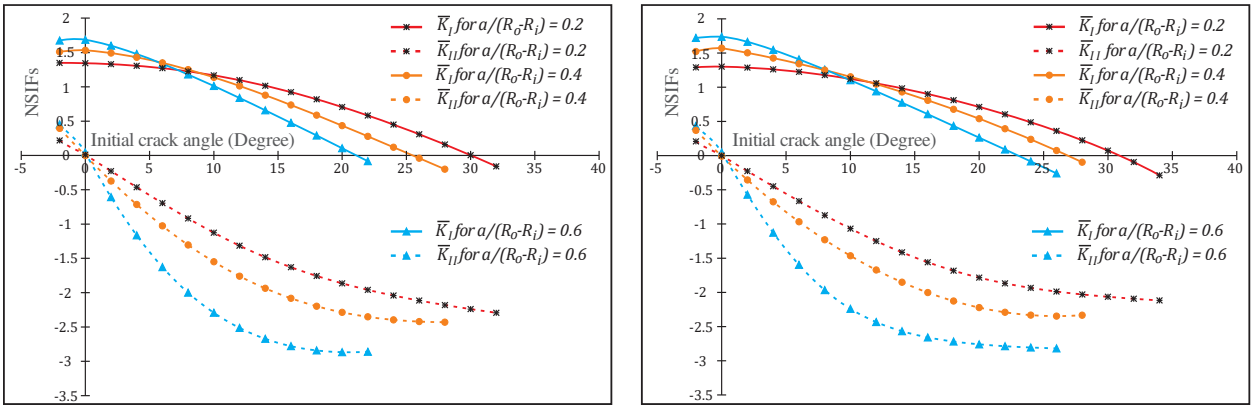

Fig. 19. NSIFs versus crack initiation angles for different crack length ratios; **a)** a homogeneous anisotropic material with $E_1/E_2=3$; **b)** an inhomogeneous ($\alpha=10$) anisotropic media with $E_1^0/E_2^0=3$.

6. Discussion and conclusions

In view of the inherent inhomogeneity and anisotropy of rocks and the absence of a comprehensive study on rock materials with such properties, this study provided an appropriate solution for the accurate simulation of such materials. For this purpose, the concept of *T*-stress was used in an anisotropic framework. In addition, inhomogeneity and anisotropy were incorporated into the calculations by the use of the *M*-integral with incompatible formulations and anisotropic crack tip enrichments functions, respectively. For validation, the NSIFs obtained from the proposed method were compared with the results of previous research works on anisotropic or inhomogeneous materials. Comparison of the results showed that the proposed method gives satisfactory results with a lower number of degrees of freedom. Furthermore, the fact that mechanical properties of a rock exposed to an acid source is a function of time and space was utilized to produce anisotropic inhomogeneous specimens. The fluorescent microscopic photographs and the extended Mori-Tanaka method were used to determine the mechanical properties at each point of the specimen. Then, the crack initiation angle and propagation trajectory obtained from the proposed XFEM analysis and the laboratory method were compared with each other. Next, a sensitivity analysis was carried out on the geometric and mechanical parameters of

anisotropic inhomogeneous HCCD specimens. The results of this study are summarized as follows:

- The results demonstrate the capability of the proposed method to estimate crack initiation angles and propagation paths, especially in the mixed mode case. Previous studies have largely neglected the inhomogeneity-anisotropy of materials and consequently, their results cannot be generalized to actual materials encountered in the field.
- The results show that not only the initial crack angle (β), but also the material orientation angle (λ) and the degree of anisotropy (E_1/E_2) have significant effects on the SIF and the crack initiation angle. In presence of such effects, using the simplifying assumption of isotropy for anisotropic materials will lead to unrealistic results.
- HCCD test configuration was used due to its simple specimen preparation process and the fact that it requires less sophisticated test apparatus. Under pure mode *I* ($\beta = 0$), this specimen experiences negligible shear stress distribution but under mixed-mode loading (e.g. with inclined crack), it experiences a significant shear stress at the crack tip, which becomes one of the main factors influencing its failure. Crack deviation from $\beta=0$ (parallel to the loading direction) disrupts the balance of stress fields near the crack tip and causes pure mode (*I*) to be turned into the mixed mode (*I/II*).
- The degree of material anisotropy (E_1/E_2) has a strong effect on Mode *I* NSIFs ($\overline{K_I}$) and the angle at which the pure mode *II* occurs (β_{II}). However, this effect is not significant on Mode *II* NSIFs ($\overline{K_{II}}$).
- When the anisotropic orientation is $\lambda=0$ and 90, the specimen will definitely experience pure mode *I* at $\beta=0$. But with any deviation of λ from these angles, β_I will diverge as well. This result shows that failure mode is a function of not only the geometric conditions but also the mechanical properties of the material. It was also found that as the degree of anisotropy (E_1/E_2) increases, material orientation angle (λ) has a significantly greater impact on $\overline{K_I}$ and $\overline{K_{II}}$ and the angle at which pure mode *I* and pure mode *II* occur (β_I and β_{II}).
- The effect of the inhomogeneity order (α) on NSIFs is not uniform but rather a function of initial crack angle (β). More specifically, deviation of the crack angle to values beyond 15° (deviation toward pure mode *I* or pure mode *II*) results in much sharper changes in NSIFs with the increase of α.

- The inhomogeneity order (α) has a mild effect on $\overline{K_I}$ and $\overline{K_{II}}$, but it will inevitably impact the failure force.
- The increase in crack length led to an increase in the pure mode *I* and *II* NSIFs. This effect was far more noticeable in $\overline{K_{II}}$, but in turn decreased the pure mode *II* angle (β_{II}).

The calculated stress intensity factors, crack initiation angles, and crack propagation paths demonstrate the capability of the proposed XFEM formulation in simulating the fracture mechanism in inhomogeneous anisotropic materials. Therefore, the study results can be used confidently in various cases (in terms of geometry, boundary conditions, and scale) for inhomogeneous anisotropic brittle materials.

References

[1] J.I. Adachi, E. Detournay, Plane strain propagation of a hydraulic fracture in a permeable rock, Engineering Fracture Mechanics, 75 (2008) 4666-4694, doi:http://dx.doi.org/10.1016/j.engfracmech.2008.04.006

[2] Q.M. Gong, Y.Y. Jiao, J. Zhao, Numerical modelling of the effects of joint spacing on rock fragmentation by TBM cutters, Tunnelling and Underground Space Technology, 21 (2006) 46-55, doi:http://dx.doi.org/10.1016/j.tust.2005.06.004

[3] G.W. Ma, X.M. An, Numerical simulation of blasting-induced rock fractures, International Journal of Rock Mechanics and Mining Sciences, 45 (2008) 966-975, doi:http://dx.doi.org/10.1016/j.ijrmms.2007.12.002

[4] E. Mohtarami, M. Eftekhari, A. Baghbanan, H. Hashemolhosseini, Chemo-Thermo-Mechanical coupling analysis of hydrocarbon reservoirs by extended finite element method, in: International conference on civil engineering, University of Tehran, Tehran, Iran, 2016, pp. 3541.

[5] E. Mohtarami, A. Jafari, M. Amini, S.M. Mazhari, Generalized Limit Equilibrium Theory for Blocky-Flexural Toppling Failure, in, International Society for Rock Mechanics.

[6] V.E. Saouma, M.-J. Kleinosky, Finite Element Simulation Of Rock Cutting: A Fracture Mechanics Approach, in, American Rock Mechanics Association.

[7] J.A. Hudson, J.P. Harrison, Engineering rock mechanics-an introduction to the principles, Elsevier, 2000.

[8] E.C. Robertson, Thermal properties of rocks, in, US Geological Survey, 1988.

[9] E. Mohtarami, A. Baghbanan, M. Eftekhari, H. Hashemolhosseini, Investigating of chemical effects on rock fracturing using extended finite element method, Theoretical and Applied Fracture Mechanics, 89 (2017) 110-126, doi:http://dx.doi.org/10.1016/j.tafmec.2017.02.003

[10] Y. Efendiev, T.Y. Hou, Multiscale finite element methods: theory and applications, Springer Science & Business Media, 2009.

[11] M. Eftekhari, A. Baghbanan, H. Hashemolhosseini, H. Amrollahi, Mechanism of fracture in macro- and micro-scales in hollow centre cracked disc specimen, Journal of Central South University, 22 (2015) 4426-4433, doi:10.1007/s11771-015-2990-z

[12] M. Eftekhari, A. Baghbanan, H. Hashemolhosseini, Fracture propagation in a cracked semicircular bend specimen under mixed mode loading using extended finite element method, Arabian Journal of Geosciences, 8 (2015) 9635-9646, doi:10.1007/s12517-015-1906-4

[13] M. Eftekhari, A. Baghbanan, H. Hashemolhosseini, Crack propagation in rock specimen under compressive loading using extended finite element method, Arabian Journal of Geosciences, 9 (2016) 145, doi:10.1007/s12517-015-2196-6

[14] M.R.M. Aliha, M.R. Ayatollahi, D.J. Smith, M.J. Pavier, Geometry and size effects on fracture trajectory in a limestone rock under mixed mode loading, Engineering Fracture Mechanics, 77 (2010) 2200-2212, doi:http://dx.doi.org/10.1016/j.engfracmech.2010.03.009

[15] S. Hirose, T. Taniguchi, F. Ouchterlony, K. Nakagawa, The Effect of Anisotropy On the KI Calibration of ISRM Standard Fracture Toughness Specimens, in: 8th ISRM Congress, International Society for Rock Mechanics, 1995.

[16] A. Asadpoure, S. Mohammadi, Developing new enrichment functions for crack simulation in orthotropic media by the extended finite element method, International Journal for Numerical Methods in Engineering, 69 (2007) 2150-2172, doi:10.1002/nme.1839

[17] H. Bayesteh, S. Mohammadi, XFEM fracture analysis of orthotropic functionally graded materials, Composites Part B: Engineering, 44 (2013) 8-25, doi:http://dx.doi.org/10.1016/j.compositesb.2012.07.055

[18] L.M.A. Cahill, S. Natarajan, S.P.A. Bordas, R.M. O'Higgins, C.T. McCarthy, An experimental/numerical investigation into the main driving force for crack propagation in uni-directional fibre-reinforced composite laminae, Composite Structures, 107 (2014) 119-130, doi:http://dx.doi.org/10.1016/j.compstruct.2013.05.039

[19] C.H. Chen, C.S. Chen, J.H. Wu, Fracture toughness analysis on cracked ring disks of anisotropic rock, Rock Mechanics and Rock Engineering, 41 (2008) 539-562, doi:10.1007/s00603-007-0152-9

[20] C.-S. Chen, E. Pan, B. Amadei, Fracture mechanics analysis of cracked discs of anisotropic rock using the boundary element method, International Journal of Rock Mechanics and Mining Sciences, 35 (1998) 195-218, doi:http://dx.doi.org/10.1016/S0148-9062(97)00330-6

[21] M. Eftekhari, A. Baghbanan, E. Mohtarami, H. Hashemolhosseini, Determination of crack initiation and propagation in two disc shaped specimens using the improved maximum tangential stress criterion, Journal of Theoretical and Applied Mechanics, 55 (2017) 469-480, doi:10.15632/jtam-pl.55.2.469

[22] C.-C. Ke, C.-S. Chen, C.-Y. Ku, C.-H. Chen, Modeling crack propagation path of anisotropic rocks using boundary element method, International Journal for Numerical and Analytical Methods in Geomechanics, 33 (2009) 1227-1253, doi:10.1002/nag.764

[23] E. Mohtarami, A. Baghbanan, H. Hashemolhosseini, Prediction of fracture trajectory in anisotropic rocks using modified maximum tangential stress criterion, Computers and Geotechnics, 92 (2017) 108-120, doi:http://dx.doi.org/10.1016/j.compgeo.2017.07.025

[24] D. Sutula, P. Kerfriden, T. van Dam, S.P.A. Bordas, Minimum energy multiple crack propagation. Part I: Theory and state of the art review, Engineering Fracture Mechanics, (2017), doi:https://doi.org/10.1016/j.engfracmech.2017.07.028

[25] D. Sutula, P. Kerfriden, T. van Dam, S.P.A. Bordas, Minimum energy multiple crack propagation. Part-II: Discrete solution with XFEM, Engineering Fracture Mechanics, (2017), doi:https://doi.org/10.1016/j.engfracmech.2017.07.029

[26] D. Sutula, P. Kerfriden, T. van Dam, S.P.A. Bordas, Minimum energy multiple crack propagation. Part III: XFEM computer implementation and applications, Engineering Fracture Mechanics, (2017), doi:https://doi.org/10.1016/j.engfracmech.2017.08.004

[27] C.C. Ke, C.S. Chen, C.H. Tu, Determination of Fracture Toughness of Anisotropic Rocks by Boundary Element Method, Rock Mechanics and Rock Engineering, 41 (2008) 509-538, doi:10.1007/s00603-005-0089-9

[28] J.-H. Kim, G.H. Paulino, The interaction integral for fracture of orthotropic functionally graded materials: evaluation of stress intensity factors, International Journal of Solids and Structures, 40 (2003) 3967-4001, doi:http://dx.doi.org/10.1016/S0020-7683(03)00176-8

[29] A. Menk, S.P.A. Bordas, Numerically determined enrichment functions for the extended finite element method and applications to bi-material anisotropic fracture and polycrystals, International Journal for Numerical Methods in Engineering, 83 (2010) 805-828, doi:10.1002/nme.2858

[30] S. Mohammadi, XFEM fracture analysis of composites, John Wiley & Sons, 2012.

[31] F. Erdogan, G.C. Sih, On the Crack Extension in Plates Under Plane Loading and Transverse Shear, Journal of Basic Engineering, 85 (1963) 519-525, doi:10.1115/1.3656897

[32] M. Hussain, S. Pu, J. Underwood, Strain energy release rate for a crack under combined mode I and mode II, in: Fracture Analysis: Proceedings of the 1973 National Symposium on Fracture Mechanics, Part II, ASTM International, 1974.

[33] R.J. Nuismer, An energy release rate criterion for mixed mode fracture, International Journal of Fracture, 11 (1975) 245-250, doi:10.1007/BF00038891

[34] G.C. Sih, Strain-energy-density factor applied to mixed mode crack problems, International Journal of Fracture, 10 (1974) 305-321, doi:10.1007/BF00035493

[35] P.S. Theocaris, N.P. Andrianopoulos, A Modified Strain-Energy Density Criterion Applied to Crack Propagation, Journal of Applied Mechanics, 49 (1982) 81-86, doi:10.1115/1.3162075

[36] P. Grassl, R. Rempling, Influence of volumetric–deviatoric coupling on crack prediction in concrete fracture tests, Engineering Fracture Mechanics, 74 (2007) 1683-1693, doi:http://dx.doi.org/10.1016/j.engfracmech.2006.08.028

[37] P. Isaksson, P. Ståhle, Mode II crack paths under compression in brittle solids – a theory and experimental comparison, International Journal of Solids and Structures, 39 (2002) 2281-2297, doi:http://dx.doi.org/10.1016/S0020-7683(02)00089-6

[38] Q. Lin, A. Fakhimi, M. Haggerty, J.F. Labuz, Initiation of tensile and mixed-mode fracture in sandstone, International Journal of Rock Mechanics and Mining Sciences, 46 (2009) 489-497, doi:http://dx.doi.org/10.1016/j.ijrmms.2008.10.008

[39] L. Song, S.M. Huang, S.C. Yang, Experimental investigation on criterion of three-dimensional mixed-mode fracture for concrete, Cement and Concrete Research, 34 (2004) 913-916, doi:http://dx.doi.org/10.1016/j.cemconres.2003.10.013

[40] G.S. Xeidakis, I.S. Samaras, D.A. Zacharopoulos, G.E. Papakaliatakis, Trajectories of unstably growing cracks in mixed mode I–II loading of marble beams, Rock Mechanics and Rock Engineering, 30 (1997) 19-33, doi:10.1007/BF01020111

[41] T. Belytschko, T. Black, Elastic crack growth in finite elements with minimal remeshing, International Journal for Numerical Methods in Engineering, 45 (1999) 601-620, doi:10.1002/(SICI)1097-0207(19990620)45:5<601::AID-NME598>3.0.CO;2-S

[42] N. Moës, J. Dolbow, T. Belytschko, A finite element method for crack growth without remeshing, International Journal for Numerical Methods in Engineering, 46 (1999) 131-150, doi:10.1002/(SICI)1097-0207(19990910)46:1<131::AID-NME726>3.0.CO;2-J

[43] J.E. Dolbow, An extended finite element method with discontinuous enrichment for applied mechanics, (2000)

[44] S. Bordas, P.V. Nguyen, C. Dunant, A. Guidoum, H. Nguyen-Dang, An extended finite element library, International Journal for Numerical Methods in Engineering, 71 (2007) 703-732, doi:10.1002/nme.1966

[45] J.E. Dolbow, M. Gosz, On the computation of mixed-mode stress intensity factors in functionally graded materials, International Journal of Solids and Structures, 39 (2002) 2557-2574, doi:http://dx.doi.org/10.1016/S0020-7683(02)00114-2

[46] A. Asadpoure, S. Mohammadi, A. Vafai, Modeling crack in orthotropic media using a coupled finite element and partition of unity methods, Finite Elements in Analysis and Design, 42 (2006) 1165-1175, doi:http://dx.doi.org/10.1016/j.finel.2006.05.001

[47] A. Asadpoure, S. Mohammadi, A. Vafai, Crack analysis in orthotropic media using the extended finite element method, Thin-Walled Structures, 44 (2006) 1031-1038, doi:http://dx.doi.org/10.1016/j.tws.2006.07.007

[48] G.C. Sih, P.C. Paris, G.R. Irwin, On cracks in rectilinearly anisotropic bodies, International Journal of Fracture Mechanics, 1 (1965) 189-203, doi:10.1007/BF00186854

[49] E. Viola, A. Piva, E. Radi, Crack propagation in an orthotropic medium under general loading, Engineering Fracture Mechanics, 34 (1989) 1155-1174, doi:http://dx.doi.org/10.1016/0013-7944(89)90277-4

[50] K. Agathos, E. Chatzi, S.P.A. Bordas, Stable 3D extended finite elements with higher order enrichment for accurate non planar fracture, Computer Methods in Applied Mechanics and Engineering, 306 (2016) 19-46, doi:https://doi.org/10.1016/j.cma.2016.03.023

[51] K. Agathos, E. Chatzi, S.P.A. Bordas, D. Talaslidis, A well-conditioned and optimally convergent XFEM for 3D linear elastic fracture, International Journal for Numerical Methods in Engineering, 105 (2016) 643-677, doi:10.1002/nme.4982

[52] K. Agathos, G. Ventura, E. Chatzi, S.P.A. Bordas, Stable 3D XFEM/vector level sets for non-planar 3D crack propagation and comparison of enrichment schemes, International Journal for Numerical Methods in Engineering, (2017), doi:10.1002/nme.5611

[53] Y. Jin, O.A. González-Estrada, O. Pierard, S.P.A. Bordas, Error-controlled adaptive extended finite element method for 3D linear elastic crack propagation, Computer Methods in Applied Mechanics and Engineering, 318 (2017) 319-348, doi:https://doi.org/10.1016/j.cma.2016.12.016

[54] M. Sheng, G. Li, D. Sutula, S. Tian, S.P.A. Bordas, XFEM modeling of multistage hydraulic fracturing in anisotropic shale formations, Journal of Petroleum Science and Engineering, 162 (2018) 801-812, doi:https://doi.org/10.1016/j.petrol.2017.11.007

[55] X. Wang, F. Shi, H. Liu, H. Wu, Numerical simulation of hydraulic fracturing in orthotropic formation based on the extended finite element method, Journal of Natural Gas Science and Engineering, 33 (2016) 56-69, doi:https://doi.org/10.1016/j.jngse.2016.05.001

[56] Q.-D. Zeng, J. Yao, J. Shao, Numerical study of hydraulic fracture propagation accounting for rock anisotropy, Journal of Petroleum Science and Engineering, 160 (2018) 422-432, doi:https://doi.org/10.1016/j.petrol.2017.10.037

[57] R.E. Gibson, Some Results Concerning Displacements and Stresses in a Non-Homogeneous Elastic Half-space, Géotechnique, 17 (1967) 58-67, doi:10.1680/geot.1967.17.1.58

[58] C. Atkinson, R.D. List, Steady state crack propagation into media with spatially varying elastic properties, International Journal of Engineering Science, 16 (1978) 717-730, doi:http://dx.doi.org/10.1016/0020-7225(78)90006-X

[59] R.S. Dhaliwal, B.M. Singh, On the theory of elssticity of a nonhomogeneous medium, Journal of Elasticity, 8 (1978) 211-219, doi:10.1007/BF00052484

[60] F. Delale, F. Erdogan, The Crack Problem for a Nonhomogeneous Plane, Journal of Applied Mechanics, 50 (1983) 609-614, doi:10.1115/1.3167098

[61] J.-H. Kim, G.H. Paulino, Finite element evaluation of mixed mode stress intensity factors in functionally graded materials, International Journal for Numerical Methods in Engineering, 53 (2002) 1903-1935, doi:10.1002/nme.364

[62] J.F. Yau, S.S. Wang, H.T. Corten, A Mixed-Mode Crack Analysis of Isotropic Solids Using Conservation Laws of Elasticity, Journal of Applied Mechanics, 47 (1980) 335-341, doi:10.1115/1.3153665

[63] S.S. Wang, J.F. Yau, H.T. Corten, A mixed-mode crack analysis of rectilinear anisotropic solids using conservation laws of elasticity, International Journal of Fracture, 16 (1980) 247-259, doi:10.1007/BF00013381

[64] B. Shen, O. Stephansson, Numerical analysis of mixed mode I and Mode II fracture propagation, International Journal of Rock Mechanics and Mining Sciences & Geomechanics Abstracts, 30 (1993) 861-867, doi:http://dx.doi.org/10.1016/0148-9062(93)90037-E

[65] N.A. Al-Shayea, Crack propagation trajectories for rocks under mixed mode I–II fracture, Engineering Geology, 81 (2005) 84-97, doi:http://dx.doi.org/10.1016/j.enggeo.2005.07.013

[66] A. Bobet, Fracture coalescence in rock materials: experimental observations and numerical predictions, in, Massachusetts Institute of Technology, 1997.

[67] B. Shen, O. Stephansson, Modification of the G-criterion for crack propagation subjected to compression, Engineering Fracture Mechanics, 47 (1994) 177-189, doi:http://dx.doi.org/10.1016/0013-7944(94)90219-4

[68] Z. Wu, L.N.Y. Wong, Frictional crack initiation and propagation analysis using the numerical manifold method, Computers and Geotechnics, 39 (2012) 38-53, doi:https://doi.org/10.1016/j.compgeo.2011.08.011

[69] D.J. Smith, M.R. Ayatollahi, M.J. Pavier, The role of T-stress in brittle fracture for linear elastic materials under mixed-mode loading, Fatigue & Fracture of Engineering Materials & Structures, 24 (2001) 137-150, doi:10.1046/j.1460-2695.2001.00377.x

[70] M.R. Ayatollahi, M.R.M. Aliha, Fracture toughness study for a brittle rock subjected to mixed mode I/II loading, International Journal of Rock Mechanics and Mining Sciences, 44 (2007) 617-624, doi:http://dx.doi.org/10.1016/j.ijrmms.2006.10.001

[71] M.R. Ayatollahi, M.R.M. Aliha, Wide range data for crack tip parameters in two disc-type specimens under mixed mode loading, Computational Materials Science, 38 (2007) 660-670, doi:http://dx.doi.org/10.1016/j.commatsci.2006.04.008

[72] M.R. Ayatollahi, M.R.M. Aliha, On the use of Brazilian disc specimen for calculating mixed mode I–II fracture toughness of rock materials, Engineering Fracture Mechanics, 75 (2008) 4631-4641, doi:http://dx.doi.org/10.1016/j.engfracmech.2008.06.018

[73] M.L. Williams, The Bending Stress Distribution at the Base of a Stationary Crack, Journal of Applied Mechanics, 28 (1961) 78-82, doi:10.1115/1.3640470

[74] M.R. Ayatollahi, M.R.M. Aliha, Mixed mode fracture in soda lime glass analyzed by using the generalized MTS criterion, International Journal of Solids and Structures, 46 (2009) 311-321, doi:http://dx.doi.org/10.1016/j.ijsolstr.2008.08.035

[75] M.R. Ayatollahi, M.J. Pavier, D.J. Smith, Determination of T-stress from finite element analysis for mode I and mixed mode I/II loading, International Journal of Fracture, 91 (1998) 283-298, doi:10.1023/A:1007581125618

[76] Z. Knésl, Evaluation of the elastic T-stress using a hybrid finite element approach, International Journal of Fracture, 70 (1994) R9-R14, doi:10.1007/BF00018140

[77] S.G. Larsson†, A.J. Carlsson, Influence of non-singular stress terms and specimen geometry on small-scale yielding at crack tips in elastic-plastic materials, Journal of the Mechanics and Physics of Solids, 21 (1973) 263-277, doi:http://dx.doi.org/10.1016/0022-5096(73)90024-0

[78] P.C. Olsen, Determining the stress intensity factors KI, KII and the T-term via the conservation laws using the boundary element method, Engineering Fracture Mechanics, 49 (1994) 49-60, doi:http://dx.doi.org/10.1016/0013-7944(94)90110-4

[79] J. Sladek, V. Sladek, P. Fedelinski, Contour integrals for mixed-mode crack analysis: effect of nonsingular terms, Theoretical and Applied Fracture Mechanics, 27 (1997) 115-127, doi:http://dx.doi.org/10.1016/S0167-8442(97)00013-X

[80] G.A. Kardomateas, R.L. Carlson, A.H. Soediono, D.P. Schrage, Near tip stress and strain fields for short elastic cracks, International Journal of Fracture, 62 (1993) 219-232, doi:10.1007/BF00012540

[81] A.H. Sherry, C.C. France, M.R. Goldthorpe, compendium of T-stress solutions for two and three dimensional cracked geometries, Fatigue & Fracture of Engineering Materials & Structures, 18 (1995) 141-155, doi:10.1111/j.1460-2695.1995.tb00148.x

[82] J.-H. Kim, G.H. Paulino, T-stress, mixed-mode stress intensity factors, and crack initiation angles in functionally graded materials: a unified approach using the interaction integral method, Computer Methods in Applied Mechanics and Engineering, 192 (2003) 1463-1494, doi:https://doi.org/10.1016/S0045-7825(02)00652-7

[83] J.-H. Kim, G.H. Paulino, T-stress in orthotropic functionally graded materials: Lekhnitskii and Stroh formalisms, International Journal of Fracture, 126 (2004) 345-384, doi:10.1023/B:FRAC.0000031092.47424.f0

[84] G.H. Paulino, J.-H. Kim, A new approach to compute T-stress in functionally graded materials by means of the interaction integral method, Engineering Fracture Mechanics, 71 (2004) 1907-1950, doi:https://doi.org/10.1016/j.engfracmech.2003.11.005

[85] S. Lekhnitskii, Theory of elasticity of an anisotropic elastic body, Holden-day, 1963.

[86] S. Mohammadi, Extended finite element method: for fracture analysis of structures, John Wiley & Sons, 2008.

[87] J.-H. Kim, G.H. Paulino, Consistent Formulations of the Interaction Integral Method for Fracture of Functionally Graded Materials, Journal of Applied Mechanics, 72 (2004) 351-364, doi:10.1115/1.1876395

[88] J.-H. Kim, G.H. Paulino, Isoparametric Graded Finite Elements for Nonhomogeneous Isotropic and Orthotropic Materials, Journal of Applied Mechanics, 69 (2002) 502-514, doi:10.1115/1.1467094

[89] V.E. Saouma, M.L. Ayari, D.A. Leavell, Mixed mode crack propagation in homogeneous anisotropic solids, Engineering Fracture Mechanics, 27 (1987) 171-184, doi:http://dx.doi.org/10.1016/0013-7944(87)90166-4

[90] C.-S. Chen, Characterization of deformability, strength, and fracturing of anisotropic rocks using Brazilian tests, in: Dept. of Civil Eng., University of Colorado, Boulder, 1996.

[91] C.-S. Chen, E. Pan, B. Amadei, Determination of deformability and tensile strength of anisotropic rock using Brazilian tests, International Journal of Rock Mechanics and Mining Sciences, 35 (1998) 43-61, doi:https://doi.org/10.1016/S0148-9062(97)00329-X

[92] N. Konda, F. Erdogan, The mixed mode crack problem in a nonhomogeneous elastic medium, Engineering Fracture Mechanics, 47 (1994) 533-545, doi:http://dx.doi.org/10.1016/0013-7944(94)90253-4

[93] J. Liu, B.H. Brady, Simulations of a coupled hydro-chemo-mechanical system in rocks, Geotechnical & Geological Engineering, 22 (2004) 121-133, doi:10.1023/B:GEGE.0000014285.21652.80

[94] E. Asadollahpour, A. Baghbanan, H. Hashemolhosseini, E. Mohtarami, The etching and hydraulic conductivity of acidized rough fractures, Journal of Petroleum Science and Engineering, 166 (2018) 704-717, doi:https://doi.org/10.1016/j.petrol.2018.03.074

[95] L. Drenchev, J. Sobczak, N. Sobczak, W. Sha, S. Malinov, A comprehensive model of ordered porosity formation, Acta Materialia, 55 (2007) 6459-6471, doi:http://dx.doi.org/10.1016/j.actamat.2007.08.008

[96] C.M. Ford, L.J. Gibson, Uniaxial strength asymmetry in cellular materials: An analytical model, International Journal of Mechanical Sciences, 40 (1998) 521-531, doi:http://dx.doi.org/10.1016/S0020-7403(97)00064-7

[97] K. Kitazono, E. Sato, K. Kuribayashi, Application of mean-field approximation to elastic-plastic behavior for closed-cell metal foams, Acta Materialia, 51 (2003) 4823-4836, doi:http://dx.doi.org/10.1016/S1359-6454(03)00322-7

[98] Y. Benveniste, A new approach to the application of Mori-Tanaka's theory in composite materials, Mechanics of Materials, 6 (1987) 147-157, doi:http://dx.doi.org/10.1016/0167-6636(87)90005-6

[99] T. Mori, K. Tanaka, Average stress in matrix and average elastic energy of materials with misfitting inclusions, Acta Metallurgica, 21 (1973) 571-574, doi:http://dx.doi.org/10.1016/0001-6160(73)90064-3

[100] J.D. Eshelby, The determination of the elastic field of an ellipsoidal inclusion, and related problems, in: Proceedings of the Royal Society of London A: Mathematical, Physical and Engineering Sciences, The Royal Society, 1957, pp. 376-396.

[101] S. Gong, Z. Li, Y.Y. Zhao, An extended Mori–Tanaka model for the elastic moduli of porous materials of finite size, Acta Materialia, 59 (2011) 6820-6830, doi:http://dx.doi.org/10.1016/j.actamat.2011.07.041

[102] F. Meraghni, C.J. Blakeman, M.L. Benzeggagh, Effect of interfacial decohesion on stiffness reduction in a random discontinuous-fibre composite containing matrix microcracks, Composites Science and Technology, 56 (1996) 541-555, doi:http://dx.doi.org/10.1016/0266-3538(96)00039-5

[103] M.L. Dunn, M. Taya, Elastic-plastic thermal stresses and deformation of short-fibre composites, Journal of Materials Science, 29 (1994) 2053-2062, doi:10.1007/BF01154679

[104] G.J. Weng, The theoretical connection between Mori-Tanaka's theory and the Hashin-Shtrikman-Walpole bounds, International Journal of Engineering Science, 28 (1990) 1111-1120, doi:http://dx.doi.org/10.1016/0020-7225(90)90111-U

[105] J. Vorel, V. Šmilauer, Z. Bittnar, Multiscale simulations of concrete mechanical tests, Journal of Computational and Applied Mathematics, 236 (2012) 4882-4892, doi:http://dx.doi.org/10.1016/j.cam.2012.01.009

[106] Q. Zhu, D. Kondo, J. Shao, V. Pensee, Micromechanical modelling of anisotropic damage in brittle rocks and application, International Journal of Rock Mechanics and Mining Sciences, 45 (2008) 467-477, doi:https://doi.org/10.1016/j.ijrmms.2007.07.014

[107] Y. Zhu, A micromechanics-based damage constitutive model of porous rocks, International Journal of Rock Mechanics and Mining Sciences, 91 (2017) 1-6, doi:https://doi.org/10.1016/j.ijrmms.2016.11.005

[108] Q. Zhu, J. Shao, Micromechanics of rock damage: Advances in the quasi-brittle field, Journal of Rock Mechanics and Geotechnical Engineering, 9 (2017) 29-40, doi:https://doi.org/10.1016/j.jrmge.2016.11.003

[109] Z. Bieniawski, I. Hawkes, International Society for Rock Mechanics Commission on Standardization of Laboratory and Field tests suggested methods for determining tensile-strength of rock materials, in, Pergamon-Elsevier science, 1978.

[110] H. Amrollahi, A. Baghbanan, H. Hashemolhosseini, Measuring fracture toughness of crystalline marbles under modes I and II and mixed mode I–II loading conditions using CCNBD and HCCD specimens, International Journal of Rock Mechanics and Mining Sciences, 48 (2011) 1123-1134, doi:http://dx.doi.org/10.1016/j.ijrmms.2011.06.015